*Int. J. Multiphase Flow* Vol. 19, No. 5, pp. 839–874, 1993
Printed in Great Britain. 

0301-9322/93 $6.00 + 0.00


# DECOMPRESSION WAVES IN FLUIDIZED BEDS

G. B. WALLIS,[1] S. P. HARVEY[1] and R. DIFELICE[2]
[1]Thayer School of Engineering, Dartmouth College, Hanover, NH 03755, U.S.A.
[2]Universita degli Studi di Genova, Genova, Italy

*(Received 17 August 1992; in revised form 19 May 1993)*

**Abstract**—A packed bed of particles may be held against the permeable roof of a fluidized column by a fluid flux that is several times the minimum fluidization flux. When the fluid flux is sufficiently reduced, particles rain down and a *decompression wave* propagates into the packed bed. We report new data of the velocity of this wave, summarize previous work and compare with new analyses. The speed of the decompression wave cannot be predicted from continuum theories that contain a mutual drag force dependent only on the relative velocity and void fraction. Several hypotheses about additional forces are used to derive theoretical values of the decompression wave velocity which are compared with data. The three most successful hypotheses, which are shown to be roughly equivalent at the higher wave speeds, include: a force proportional to the second derivative of void fraction; a discrete averaging method over distances scaled by particle size; and a modification to the drag force using the geometrical relationship between area fraction and number density.

*Key Words:* fluidization, waves, constitutive equations, stability, averaging

## 1. INTRODUCTION

Fluidized bed technology is widely used in many engineering applications. The phenomenon of fluidization can be visualized in terms of a simple experiment in which a bed of solid particles is supported on a porous plate in a vertical tube. Gas or liquid is forced to flow upwards through the plate and through the particle bed. This flow causes a pressure drop across the bed and when this pressure drop is sufficient to support the weight of the particles, the bed is said to be incipiently fluidized and the "minimum fluidization flux" (volumetric flow rate divided by the tube's cross-sectional area) is $j_{mf}$. A further increase in the flow causes the bed to expand. The fluidized bed thus formed has many of the properties of a liquid; its upper surface remains horizontal when the containing apparatus is tilted; and it hardly impedes the movement of objects within it or floating on the surface. If the flow of gas or liquid is increased still further, to the point at which the flow velocity becomes greater than the free-falling velocity of the particles, $v_\infty$, they are carried out of the apparatus.

In a fluidized bed, particles are suspended in a stream of moving fluid, and buoyancy and drag forces combine to balance the weight of the particles. If the velocities are relatively low and the duct sufficiently large, wall friction may be neglected and the relative motion is thus only a function of the local concentration, system properties and the gravitational field. For a uniformly fluidized suspension in one-dimensional vertical motion, the balance between forces due to gravity, drag and pressure gradient has been represented by various recipes over the years (e.g. Richardson & Zaki 1954; Simpson & Rodger 1961; Wen & Yu 1966; Wallis 1969, 1977; Gibilaro *et al.* 1985). However, it has been predicted for decades (e.g. Murray 1965; Jackson 1963; Wallis 1969) that fluidized beds that are only subject to such forces are inherently unstable and will operate in some intermittent non-uniform regime, often characterized by "bubbles" of fluid surrounded by a more-or-less uniform, but agitated, dispersion. Since some fluidized beds do operate in a very uniform, regular fashion, several authors have speculated about mechanisms to produce this stability (e.g. Jackson 1963; Wallis 1962; Foscolo & Gibilaro 1984; Batchelor 1988). While some of these approaches are partially successful at predicting the stability limits of uniform fluidization, no definitive and convincing proof of the mechanisms *per se* has yet been presented.

A related problem is how to express the basic conservation laws for non-uniform or intermittent motion of particle dispersions. Various "forces" have been postulated and estimated in the

momentum balances and occasionally there have been attempts to correct the continuity equation (Singh & Joseph 1991), but there is a very small basis of experimental data that unequivocally tests and quantifies these various hypotheses or predictions.

This paper is concerned with a particular phenomenon, easily set up in a laboratory, that existing theories have difficulty predicting. This "decompression wave" occurs when particles detach and "rain down" from the bottom of a close-packed region which may either be held stationary against a grid or may be moving as a "slug" in a naturally intermittent fluidized bed. Within this wave there usually are:

- Large changes in void fraction over lengths comparable with the particle size.
- Significant inertial effects.
- Regions where the net forces on the particles, predicted by the usual "drag" correlations, together with buoyancy and gravity, act in a direction opposite to the particle acceleration.

After describing this experiment and some data, we will examine several hypotheses that have varying success at explaining them.

## 2. DECOMPRESSION WAVES

We consider (figure 1) an initial state in which a stack of particles is held against the permeable top of a vertical column by a large upwards flux of fluid.

The fluid flux is then suddenly reduced and held constant at a given value $j_{fa}$. If $j_{fa}$ is sufficiently low, yet high enough to maintain the stack packed against the permeable grid, particles are able to fall from the bottom layer of the stack. As particles fall off the bottom of the stack, the interface between the falling particle region and the packed section propagates upwards at more or less constant velocity, $v_{dw}$, which will be called the "decompression wave velocity". In our experiments, this velocity was determined by timing the interface between two marks on the tube set 300 mm apart.

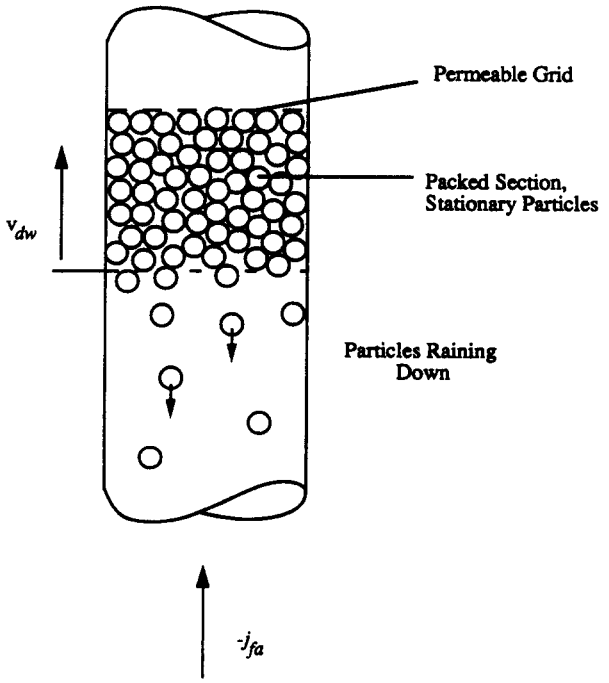


Figure 1. Sketch of decompression wave propagation.

Experimentally, it is observed that decompression waves occur as described for

$$j_{mf} \leqslant j_{fa} \leqslant \gamma j_{mf}.$$

Empirically, $\gamma$ varies within the range 1.4 to around 3.

If $j_{fa} < j_{mf}$, the whole packed section falls, whereas if $j_{fa} > \gamma j_{mf}$, there is no movement.

Our experimental apparatus is illustrated in figure 2 and had as its major features a test section made from cast plexiglass tubing, 76 mm i.d. and 1.5 m long, delimited by two stainless-steel mesh retaining grids. It was preceded by a 300 mm long calming section. In order to enable the experiment to be prepared (i.e. stacking the particles against the permeable top of the column) without resorting to high fluid flow rates, the entire section could be inverted by pivoting about its middle. Further details are given by Harvey (1991).

The minimum fluidization velocity was estimated in two ways: in the usual manner, from visual observation of initial bed expansion; and also by noting the fluid velocity at which the decompression wave experiment gave rise to an initial downwards movement of the entire packed section. Good agreement was found between these alternative methods. It was found that the maximum "allowable" particle size was 8 mm. Larger particles tended to get jammed in the tube as a result of their diameters being relatively large compared to the tube diameter.

A typical plot of the decompression wave velocity $v_{dw}$ as a function of the relative flow rate $j_{fa}/j_{mf}$ is shown in figure 3. The gap in the data for low fluid fluxes is due to the practical difficulties associated with visual tracking of waves moving at such high velocities.

For large particles (higher Reynolds numbers), the interface was observed to remain horizontal and propagate upwards at an essentially constant velocity, whereas with smaller particles, behavior tended to be more complicated: three-dimensional effects such as swirling and churning appeared; the interface was no longer horizontal and the wave velocity became irregular. These irregularities

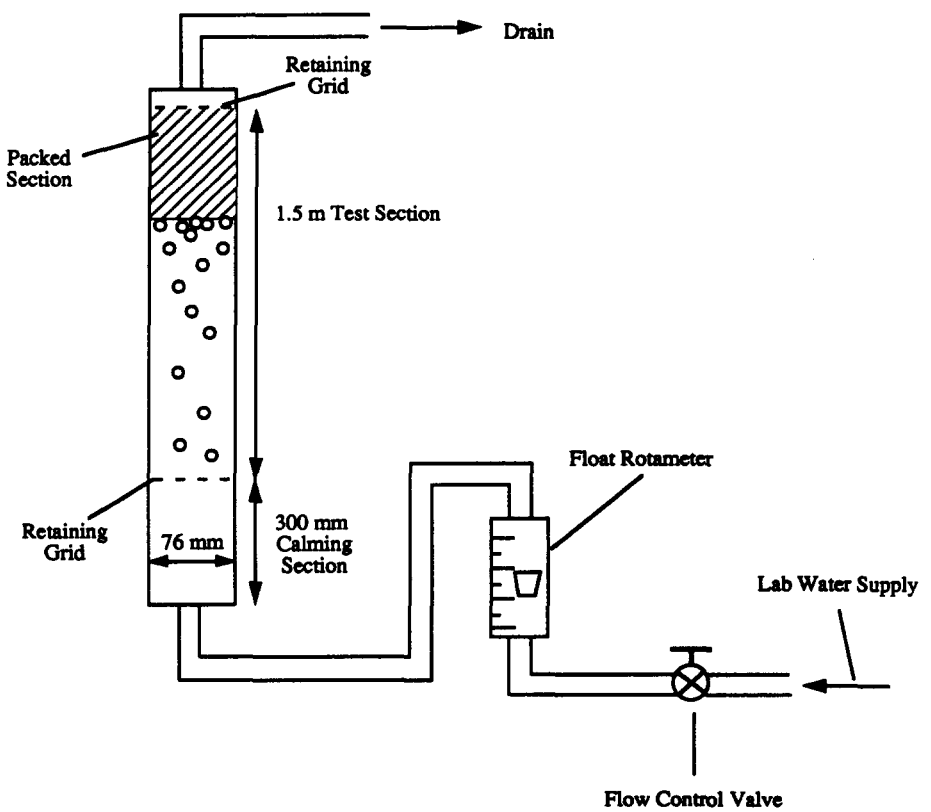


Figure 2. Experimental setup.

could be partly reduced by setting up the experiment so that a fluidized bed existed in the lower parts of the tube with the top of its surface close to the bottom of the stack.

Wallis (1962) performed similar experiments three decades ago in an effort to measure the effective "compressibility" of a fluidized suspension and relate it to the stability of uniform fluidization. He plotted his results in dimensionless form using semi-logarithmic coordinates (figure 4; the index "$a$" appearing in the abscissa on this graph is defined in [9]) and was particularly interested in the limiting behavior near $j_{fa}/j_{mf} = 1$. A similar approach was taken in a series of experiments by Gibilaro *et al.* (1989, 1990).

During a sojourn at University College, London in 1990, one of the authors (R. DiFelice) obtained the data shown in figure 5. The systems consisted of spherical particles of various materials and diameters fluidized by water. The decompression wave speed was made dimensionless by dividing by $v_\infty$, the terminal speed of a single particle falling in a stationary fluid. The open symbols and the data for lead shot correspond to one-dimensional behavior with a clear wave front. The closed symbols represent much more irregular multi-dimensional behavior and are an average of the speed of the location at which some particle motion was first detected over a long length of the tube.

In the apparatus sketched in figure 2, Harvey (1991) performed experiments with glass spheres of diameter 8, 6, 2, 1 and 0.42 mm in water, spanning the range from completely one-dimensional to mostly multi-dimensional behavior.

The data that we have examined are generally consistent with each other. Moreover, dimensional analysis suggests that only two additional parameters (e.g. $\rho_s/\rho_f$, the density ratio, and the Reynolds number for a single particle falling in an infinite fluid, $\mathrm{Re}_\infty$) are needed to correlate data such as that presented in figure 5. Therefore, the quest for a comprehensive explanation would appear to have a fair chance of success. Our various explorations along the way will now be described.

## 3. THEORY

### 3.1. General

The starting point for analysis will be the one-dimensional equations for conservation of mass and momentum for incompressible phases given by Wallis (1969). Since we shall analyze waves in a coordinate system which brings them to rest, we only need the steady-flow versions. Later, modifications will be considered which may be appropriate.

The continuity equations are

$$j_s = v_s(1 - \varepsilon) \qquad [1]$$

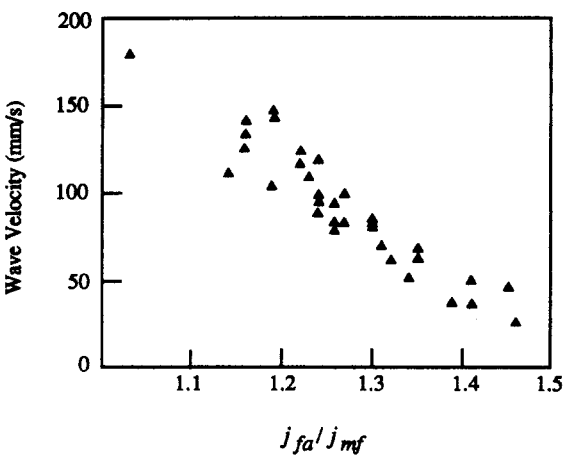


Figure 3. Decompression wave: typical data (8mm soda glass particles).

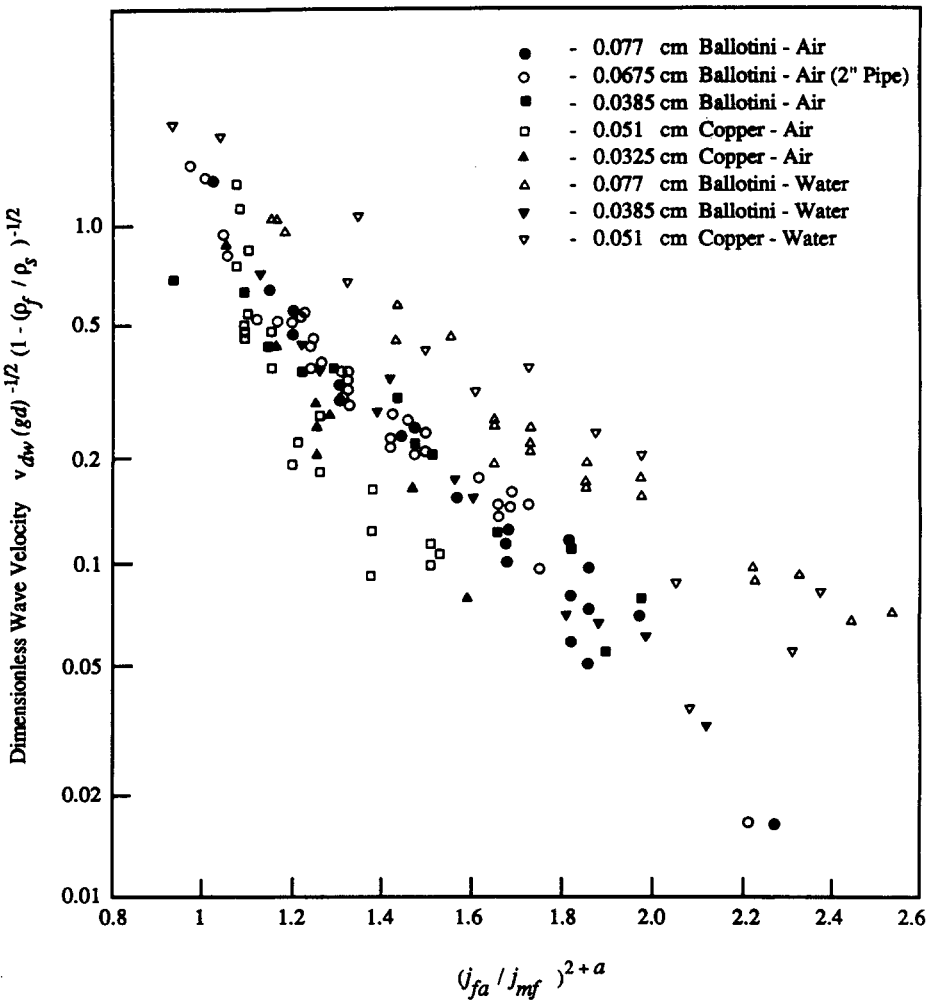


Figure 4. Data of Wallis (1962). The index $a$ is defined in [9]. The ballotini were glass balls and all the particles were nominally spherical.

and

$$j_f = v_f \varepsilon, \tag{2}$$

and the equations of motion are written as

$$\rho_s v_s \frac{dv_s}{dz} = -\frac{dp}{dz} + g\rho_s + f_s \tag{3}$$

and

$$\rho_f v_f \frac{dv_f}{dz} = -\frac{dp}{dz} + g\rho_f + f_f. \tag{4}$$

The "pressure" appearing in [3] and [4] is a suitable mean pressure in the fluid as measured, for example, by a pressure tap; in general, its gradient produces similar effects on both phases. All fluid dynamic forces that are not contained in $dp/dz$ appear in $f_f$ and $f_s$; the commonest of these are "mutual" forces which act in opposite directions on the phases. A recipe for these mutual forces in a steady fluidized bed composed of spherical particles is given by Wallis (1969) as

$$\frac{f_s}{\varepsilon} = -\frac{f_f}{1-\varepsilon} = C_{Ds}\frac{3}{4}\rho_f \varepsilon^{-2.7}\frac{(v_f - v_s)|v_f - v_s|}{d}, \tag{5}$$

where $C_{Ds}$ is a function of a Reynolds number,

$$\mathrm{Re}_s = \frac{\rho_f \varepsilon |v_f - v_s| d}{\mu_f}, \qquad [6]$$

and a typical correlation is

$$C_{Ds} = \frac{24}{\mathrm{Re}_s}(1 + 0.15\mathrm{Re}_\infty^{0.687}); \quad \mathrm{Re}_s < 1000 \qquad [7]$$

and

$$C_{Ds} = 0.44, \qquad \mathrm{Re}_s > 1000. \qquad [8]$$

Alternatively, a fit may be achieved over a limited range in the form

$$C_{Ds} = A\,\mathrm{Re}_s^a, \qquad [9]$$

where "$a$" depends on $\mathrm{Re}_s$.

This mutual drag force is not the only "component" of $f_f$ and $f_s$. Indeed, later paragraphs will feature hypotheses about additional terms (which cannot necessarily be treated as linearly additive). For the moment we proceed by subtracting [4] from [3] and including an estimate of the "added mass" effects from potential flow theory (Wallis 1990) to obtain

$$(\rho_s + C\rho_f)v_s \frac{\mathrm{d}v_s}{\mathrm{d}z} - (\rho_f + C\rho_f)v_f \frac{\mathrm{d}v_f}{\mathrm{d}z} = g(\rho_s - \rho_f) + \frac{3}{4}\varepsilon^{-2.7} C_{Ds}\rho_f \frac{(v_f - v_s)|v_f - v_s|}{d} + \text{etc.}, \qquad [10]$$

where $C = 1/2$ for spheres. If $\rho_s \gg \rho_f$, it may be sufficient to consider only the inertia term for the solids on the left-hand side (LHS) of [10], which then resembles the equation of motion [3] with [4] used to evaluate $\mathrm{d}p/\mathrm{d}z$.

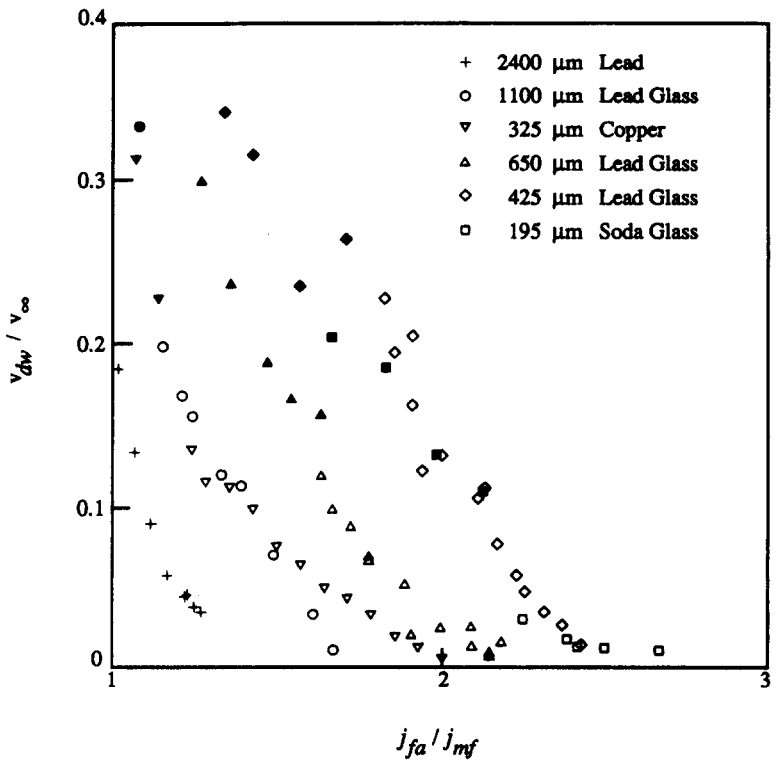


Figure 5. Data of R. DiFelice (personal communication). Solid symbols indicate three-dimensional behavior.

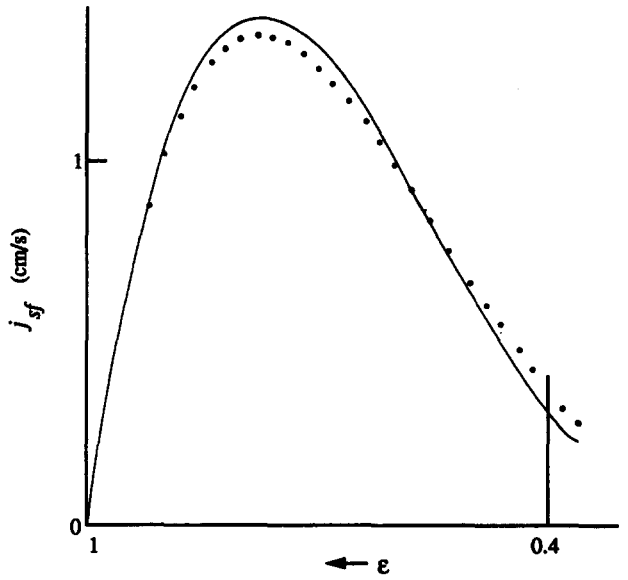


Figure 6. Drift flux curve for 325$\mu$m copper spheres in water at 10°C: ——, [10]; ····, [14] with $v_\infty = 14.6$cm/s, $n = 3.5$.

The expansion characteristics of a uniform fluidized bed in steady state may be derived from [10] by putting the LHS to zero. The particles are at rest ($v_s = 0$) and the fluid flux is given by [2]; therefore, if [9] is used, we obtain

$$g(\rho_s - \rho_f) = \frac{3}{4} A \left(\frac{\rho_f |j_f| d}{\mu_f}\right)^a \rho_f \varepsilon^{-4.7} \frac{(-j_f)|j_f|}{d}, \qquad [11]$$

where $j_f$ is negative. The result of rearranging [11] is

$$-j_f = v_\infty \varepsilon^{4.7/(2+a)}, \qquad [12]$$

where $v_\infty$ is the terminal velocity of a single particle and is equal to $(-j_f)$ when $\epsilon = 1$. Equation [12] has the form of the Richardson & Zaki (1954) correlation, in which the index is expressed as

$$n = \frac{4.7}{2+a}. \qquad [13]$$

It may also be written in terms of the "drift flux"

$$j_{sf} = j_s \varepsilon - j_f(1-\varepsilon) = v_\infty (1-\varepsilon)\varepsilon^n, \qquad [14]$$

which represents the volumetric flux of the solid phase (or minus the volumetric fluid flux) relative to the overall flux:

$$j = j_s + j_f. \qquad [15]$$

Figure 6 shows the drift flux for copper spheres, 325 $\mu$m dia, computed from [10] using [7] and [8], or fitted by [14] with $v_\infty = 14.6$ cm/s, $n = 3.5$. The curves stop close to $\varepsilon = 0.4$, where the particles rest on one another. From the form of [10] we can see that when the drift flux exceeds the value on the curve in figure 6 at a given $\varepsilon$, the net hydrodynamic force on the particles will exceed their buoyant weight; while the converse will be true below the curve.

We will now proceed to analyse decompression waves using different assumptions about the "force" terms.

### *3.2. Continuity waves*

Continuity (kinematic) waves are one-dimensional phenomena governing transient behavior when inertial effects can be neglected, either because they are small or because they are damped

out by viscous dissipation. They are quasi-equilibrium phenomena, implying that the balance of forces in the wave is essentially the same as it is in a uniform suspension under the same local conditions. Gradients, and higher derivatives, of properties such as velocity and concentration exert no influence. Continuity wave theory is a well-established way of analyzing sedimentation and foam drainage phenomena as well as many transients and limiting conditions in bubble columns and fluidized beds.

For a uniformly fluidized suspension in one-dimensional vertical motion, the balance between forces due to gravity, drag and pressure gradient can be represented by the equilibrium drift flux, as in [14].

The speed of continuity waves (Wallis 1969) is

$$v_w = j - \frac{dj_{sf}}{d\varepsilon} \qquad [16]$$

and the speed of finite discontinuities (continuity shocks) between states "1" and "2" is

$$v_s = j - \frac{(j_{sf})_1 - (j_{sf})_2}{\varepsilon_1 - \varepsilon_2}, \qquad [17]$$

where the overall flux, $j$, that is independent of $z$ in an incompressible system with no phase change or reaction, is given by [15].

Equations [16] and [17] both have simple graphical interpretations on a plot of $j_{sf}$ vs $\varepsilon$.

For hard particles, [14] is only valid at void fractions above a critical value $\varepsilon_0$ ($\sim 0.4$ for spheres) at which the particles randomly pack together. Particle–particle forces in a stationary packed assembly make it possible for the resultant force from the fluid to differ from the weight of the particle, exceeding it if $j_{sf}$ exceeds the value given by [14], with $\varepsilon = \varepsilon_0$.

Using [14], we may explicitly evaluate the second term in [16] as

$$\frac{dj_{sf}}{d\varepsilon} = v_\infty \varepsilon^{n-1}[n(1-\varepsilon) - \varepsilon]. \qquad [18]$$

For systems of uniform spherical particles, $n$ varies in the range 2.35–4.7, depending on the Reynolds number of the relative motion.

In what follows we will make all velocities dimensionless by dividing by $v_\infty$, thus:

$$j_s^* = \frac{j_s}{v_\infty}, \quad v_w^* = \frac{v_w}{v_\infty} \quad \text{etc.} \qquad [19]$$

### *3.3. Decompression waves from continuity wave theory*

We consider an initial state in which a stack of packed particles is held against the permeable top of a vertical column by a large upward flux of fluid. The fluid flux is then suddenly reduced and held constant at a (negative) value $j_{fa}$ at which particles are able to fall from the bottom of the stack. In the stack itself we have $j_s = 0$, $j_f = j_{fa}$, $\varepsilon = \varepsilon_0$ and the "state" is represented by point "$a$" in figure 7.

At the bottom of the stack the entire range of void fractions from $\varepsilon = \varepsilon_0$ to $\varepsilon = 1$ are initially present and each will try to propagate at the speed given by [16]. Since the lowest concentrations propagate (downwards) the fastest, they will escape from those following them and form an expansion wave with its leading edge moving at a speed equal to $v_\infty + j_{fa}$.

In order to complete the range of $\varepsilon$ from $\varepsilon = 1$ down to $\varepsilon = \varepsilon_0$, there must be a "shock" from point "$a$" to some point on the curve. If this point is to the left of the point of contact of the tangent from "$a$" to the curve (at $\varepsilon = \varepsilon_1$), part of the shock will break off as an expansion wave, moving the point representing the state below the shock to the right. On the other hand, if this point is to the right of the contact point, continuity waves adjacent to the shock will catch up with it until the one below the shock is moving at exactly the shock speed, i.e. the shock is represented by a tangent to the curve. We conclude that the states in the expansion wave and at the end of the shock must be as indicated in figure 7. The corresponding profile of $\varepsilon$ vs $z$ is shown in figure 8. There is one wave, with $\varepsilon = \varepsilon_2$, which is actually stationary since the two terms in [16] cancel.

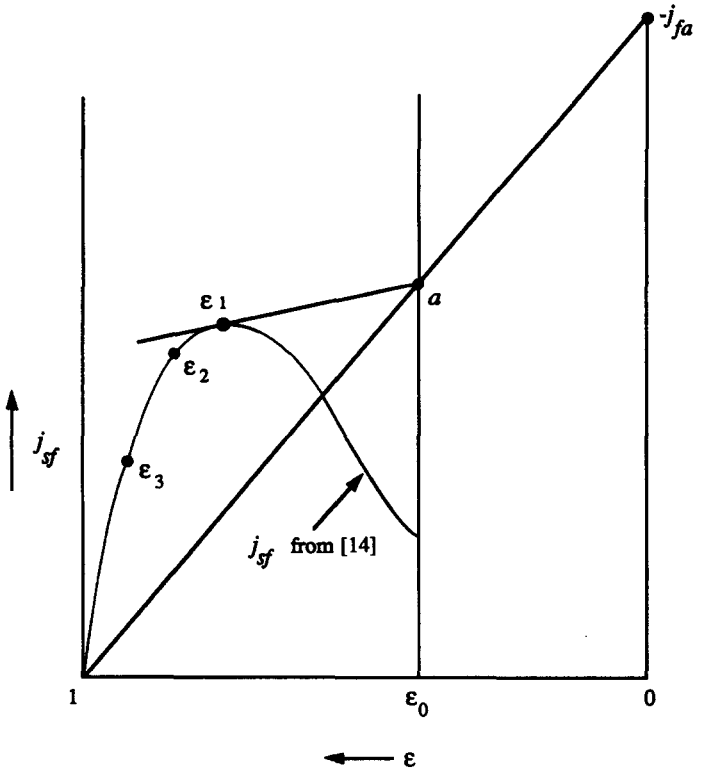


Figure 7. "States" in the drift flux diagram.

We define the velocity of the "decompression wave" as the velocity with which the top of this wave structure propagates into the stack of stationary particles. For the situation illustrated in figure 8, this is the velocity of the shock from $\varepsilon = \varepsilon_1$ to point "$a$". If $n < 2.33$, which apparently never happens for fluidized beds of uniform spherical particles, the limiting case as $j_{fa}$ approaches $j_{mf}$, the minimum fluidization flux, is the continuity wave velocity at $\varepsilon = \varepsilon_0$. Normally, the velocity is more negative (larger speed) because the shock has a steeper negative slope.

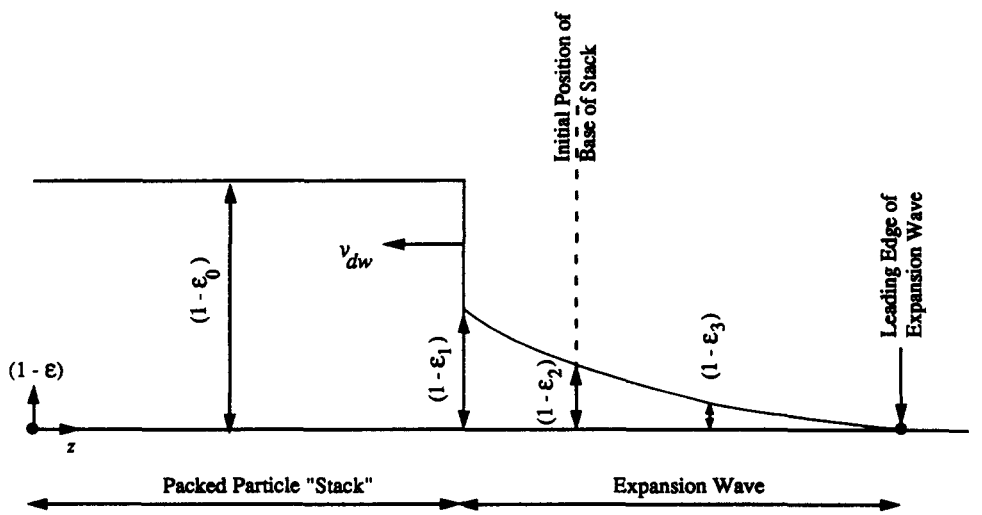


Figure 8. Instantaneous particle concentration profile.

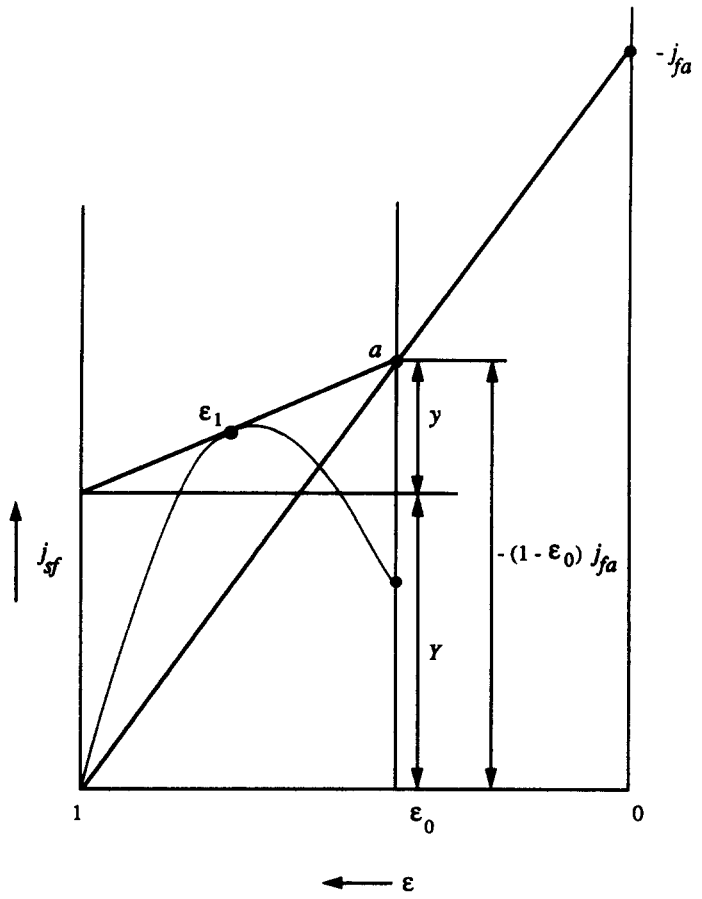


Figure 9. Graphical construction to determine $Y$ in [20].

The decompression wave velocity can be straightforwardly derived by analytic or geometrical methods. Referring to the parameters indicated in figure 9, the shock velocity from "$a$" to $\varepsilon = \varepsilon_1$ is

$$\begin{aligned} v_s &= j_{fa} + \text{slope of the shock line} \\ &= j_{fa} + \frac{y}{1-\varepsilon_0} \\ &= \frac{-[-(1-\varepsilon_0)j_{fa} - y]}{1-\varepsilon_0} = \frac{-Y}{1-\varepsilon_0}, \end{aligned} \qquad [20]$$

which is easily constructed graphically. Since $Y$ is positive, the wave speed is negative; i.e. the wave moves upwards.

An analytical solution may be obtained using $\varepsilon_1$ as a parameter. From geometry and use of [14] and [17], we get

$$\begin{aligned} Y^* &= j^*_{sf} + (1-\varepsilon_1)\frac{\mathrm{d}j^*_{sf}}{\mathrm{d}\varepsilon_1} \\ &= n(1-\varepsilon_1)^2\varepsilon_1^{n-1}, \end{aligned} \qquad [21]$$

$$-j^*_{fa} = \frac{Y^*}{1-\varepsilon_0} + \varepsilon_1^{n-1}[n(1-\varepsilon_1) - \varepsilon_1] \qquad [22]$$

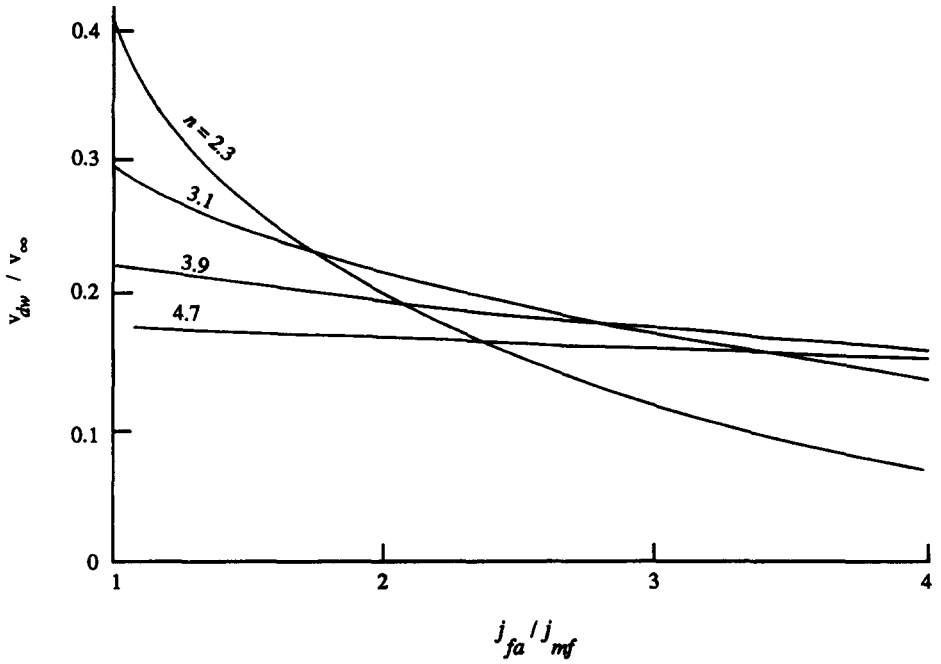


Figure 10. Prediction of decompression wave speed from continuity wave theory for various values of $n$.

and

$$v_s^* = v_{dw}^* = -\frac{Y^*}{1-\varepsilon_0}. \qquad [23]$$

The dimensionless minimum fluidization flux follows from [14] with $j_s = 0$ and $\varepsilon = \varepsilon_0$,

$$-j_{mf}^* = \varepsilon_0^n. \qquad [24]$$

These equations were used to construct a plot of $v_{dw}^* = v_{dw}/v_\infty$ vs $j_{fa}/j_{mf} = j_{fa}^*/j_{mf}^*$ for a series of values of $n$ (figure 10). When these results are compared with data, such as was presented in figure 5, it is found that decompression waves which appear one-dimensional always propagate slower than would be predicted from continuity wave theory. Decompression waves which propagate faster than this theory predicts are all multi-dimensional in character.

Since one-dimensional decompression waves propagate slower than the maximum speed set by continuity wave theory, some other effects must influence their motion. Before investigating several hypotheses about such effects, we will present a qualitative analysis of what some of their properties must be.

### *3.4. Other effects*

Continuity wave theory ignores inertia effects and the influences of property gradients. This is justifiable as long as the wave is "long" and overall balances can be made between quasi-equilibrium states on either side of it. Of course, inertia is always present and complete force balances must contain a component to account for it. From another point of view, states which do not line on the $j_{sf}$ curve, representing a balance between gravity and drag, must be subject to other forces or inertia effects which complete the momentum balance.

This logic may be applied qualitatively to the theory in the previous section. It is easiest to analyze the situation after the wave has developed for some time and conditions are "steady" in a coordinate system moving with the wave speed.

It is still possible to represent the entire wave as a transition from some state "$a$" in the compacted particle stack to another "equilibrium" steady state "$c$" far below where the forces are

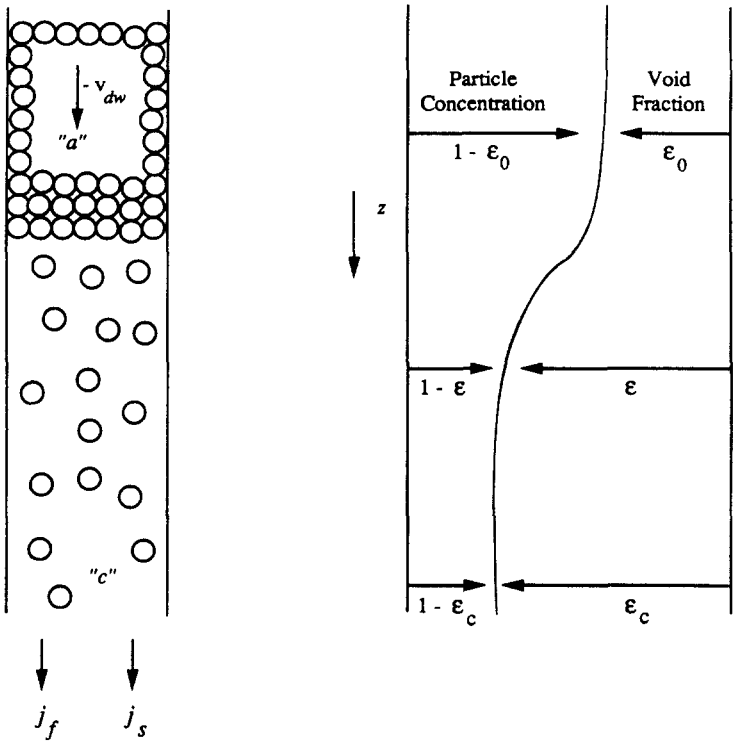


Figure 11. Steady flow relative to the wave.

again in balance. Equation [17], between these states, still describes the wave speed. In reality this "jump" must have an internal structure on a suitably small scale.

For convenience, a steady flow situation is achieved by imposing a velocity—$v_{dw}$ on the situation considered before (figure 11). The overall flux is now

$$j = j_{fa} - v_{dw}. \qquad [25]$$

The flux of solids is

$$j_s = -v_{dw}(1 - \varepsilon_0) \qquad [26]$$

and the fluid flux is

$$j_f = j_{fa} - \varepsilon_0 v_{dw}. \qquad [27]$$

We are still using the convention that the positive direction is given by $v_\infty$ and will be downwards for $\rho_s > \rho_f$.

Since all of these fluxes are constant, in this steady flow situation, only one independent variable is needed to define the local state and may be chosen as $\varepsilon$. The phase velocities are

$$v_s = \frac{-v_{dw}(1 - \varepsilon_0)}{1 - \varepsilon} \qquad [28]$$

and

$$v_f = \frac{j_{fa}}{\varepsilon} - \frac{\varepsilon_0 v_{dw}}{\varepsilon} \qquad [29]$$

and the drift flux is

$$j_{sf} = j_s\varepsilon - j_f(1 - \varepsilon) = j_s - j(1 - \varepsilon) = -v_{dw}(1 - \varepsilon) - j(1 - \varepsilon). \qquad [30]$$

As $\varepsilon$ varies, the drift flux depends linearly on $\varepsilon$ and may be represented on the $(j_{sf}, \varepsilon)$ plane as a straight line (figure 12). The states within the wave (no longer regarded as a discontinuity, but

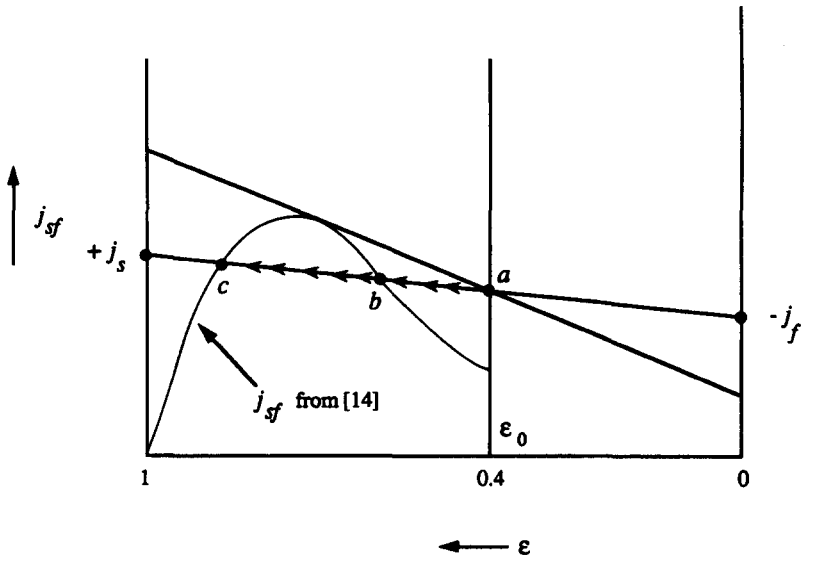


Figure 12. The series of "states" in the wave.

magnified to reveal its structure) proceed along this straight line from the packed bed at "$a$" to another uniform state "$c$", below the wave, which lies on the force balance curve described by [14]. The largest possible value of $-v_{dw}$ ($v_{dw}$ is negative) is obtained where [30] is a tangent to this curve, as derived previously. If there are other limiting factors (as experimental evidence indicates) the wave speed will be less and [30] will cut the curve twice, at "$b$" and "$c$" in the figure.

It is now pertinent to inquire how the local momentum balance works out at points in the wave. In a uniform flow, drag forces increase with $j_{sf}$, at constant $\varepsilon$; therefore, at points lying above the curve in figure 12 the net force on a particle will be upwards (for $\rho_s > \rho_f$). Along the portion $ab$ of the line representing the series of states in the wave the net force is therefore in a direction opposite to the particle acceleration, a situation that is physically incongruous and can only be legitimized by the intervention of some other "force". While several candidate forces have been hypothesized, none has yet been clearly established as existing. In view of the behavior of continuity waves at the lower end of the overall expansion wave, it is likely that the region of uniform flow below the wave will correspond to point "$c$", but the "potential barrier" in the region $ab$ must somehow be overcome on the way.

### *3.5. Force proportional to $d\varepsilon/dz$—hypothesis 1*

One candidate for the role of supplementary force mentioned above is an effective compressibility of the particle matrix manifested as a force on particles in a void fraction gradient. Several phenomena could contribute to such an effect, including particle–particle forces, fluctuations in particle motion and effects on drag due to relative acceleration (which can be estimated for the high Re case using boundary layer theory). Any effect of hydrodynamic origin must also depend on the relative motion and other "objective" parameters that are independent of the coordinate system.

If there is a "force due to voidage gradient" which can be added to the drag force in [10] (at best a first approximation but not implying any general principle of superposition), the latter, with fluid inertia ignored, takes the form

$$\rho_s v_s \frac{dv_s}{dz} = g(\rho_s - \rho_f) - \varepsilon^{-2.7} C_{Ds} \frac{3}{4} \rho_f \frac{(v_s - v_f)|v_s - v_f|}{d} + k \frac{d\varepsilon}{dz}, \qquad [31]$$

where $k$ is positive and depends on $\varepsilon$, $(v_s - v_f)$ and so on.

Since $v_s$ and $v_f$ are both derivable as functions of $\varepsilon$ from [17] and [2], [31] becomes a differential equation to be solved for $\varepsilon$. Using [1] on the LHS, we obtain

$$\frac{d\varepsilon}{dz} = \frac{g(\rho_s - \rho_f) - \varepsilon^{-2.7} C_{Ds} \frac{3}{4} \rho_f (v_s - v_f)|v_s - v_f|}{\frac{\rho v_s^2}{1-\varepsilon} - k}. \quad [32]$$

The numerator in [32] is the difference between gravitational and viscous effects referred to previously. The presence of $k$ in the denominator allows the sign to change depending on the relative magnitudes of $v_s^2$ and

$$c^2 = \frac{k(1-\varepsilon)}{\rho}, \quad [33]$$

which plays the role of the square of the "compressibility wave speed". Indeed [32] has the same form as the "backwater curve" equation in open channel flows and analogous equations for compressible flow in ducts.

This theory now offers an explanation of how the "state" can pass continuously from "$a$" to "$c$" in figure 12. In the region $ab$, $v_s^2 < c^2$, the denominator is negative, the numerator is negative because drag exceeds weight, and $d\varepsilon/dz$ is positive, as required. At the point "$b$" both the numerator and denominator are zero, corresponding to a critical condition. In the region $bc$, $v_s^2 > c^2$, the denominator is positive, the numerator is positive and $d\varepsilon/dz$ remains positive.

In the limiting condition where point "$a$" lies on the equilibrium drift flux curve (i.e. $j_{fa} = j_{mf}$), points "$a$" and "$b$" coincide at the critical condition. Moreover, from [28], $v_s = -v_w$ and we conclude that $v_w^2 = c^2$, indicating that the dynamic wave speed can be measured by a decompression wave experiment performed with a fluid flux equal to the minimum fluidization flux, an assertion made many years ago (Wallis 1962), but not put into explicit mathematical form.

One reasonable hypothesis about the form of "$k$" is that the hydrodynamic forces due to voidage gradient should be proportional to the steady flow value. In this case the interaction force in [10] becomes

$$f_s - f_f = -\varepsilon^{-2.7} C_{Ds} \frac{3}{4} \rho_f \frac{(v_s - v_f)|v_s - v_f|}{d} \left(1 - kd \frac{d\varepsilon}{dz}\right). \quad [34]$$

The inclusion of the factor "$d$" in the final term is justified by considerations of geometrical similarity. When [34] is used in place of the corresponding terms in [31] and both the numerator and denominator of the resulting equivalent of [32] are equated to zero at the critical point, we obtain

$$v_s^2 = c^2 = \frac{k(1-\varepsilon) dg(\rho_s - \rho_f)}{\rho_s}, \quad [35]$$

resembling some expressions to be found in the literature, having $k$ of the order of 1. Equation [35] appears consistent with data near the minimum fluidization point in figure 4.

Equation [32] is a differential equation for $\varepsilon$ which can be solved numerically to obtain the wave shape. In order for the solution to proceed continuously through the critical point "$b$", the numerator and denominator must pass through zero simultaneously. One solution strategy, therefore, is to assume reasonable values of $j_s$ and $j_f$ in the frame of reference which brings the wave to rest, start the solution at $z = 0$, $\varepsilon = \varepsilon_0$, and integrate forward in $z$. If $j_f$ is too low, for a given $j_s$, the denominator is found to go to zero before the numerator and the solution "blows up" before $b$ is reached. On the other hand, too high a value of $j_f$ makes the numerator zero first and the solution stops at $b$ with no further changes. Only a certain value of $j_f$ at given $j_s$, allows continuous passage through state "$b$" and on to state "$c$". A typical solution for copper spheres of 325 $\mu$m dia in water at 10°C and $k = 0.43$, $j_s = 1.5$ cm/s, $j_f = 0.447$ cm/s is shown in figure 13 and the solution is developed to greater values of $z$ in figure 14. For these conditions we may use [24]–[26] to obtain $j_{fa}/j_{mf} = 1.14$ and $v_{dw}/v_\infty = 2.5/14.6 = 0.171$, which is about 70% of the wave speed predicted by continuity wave theory under the same conditions.

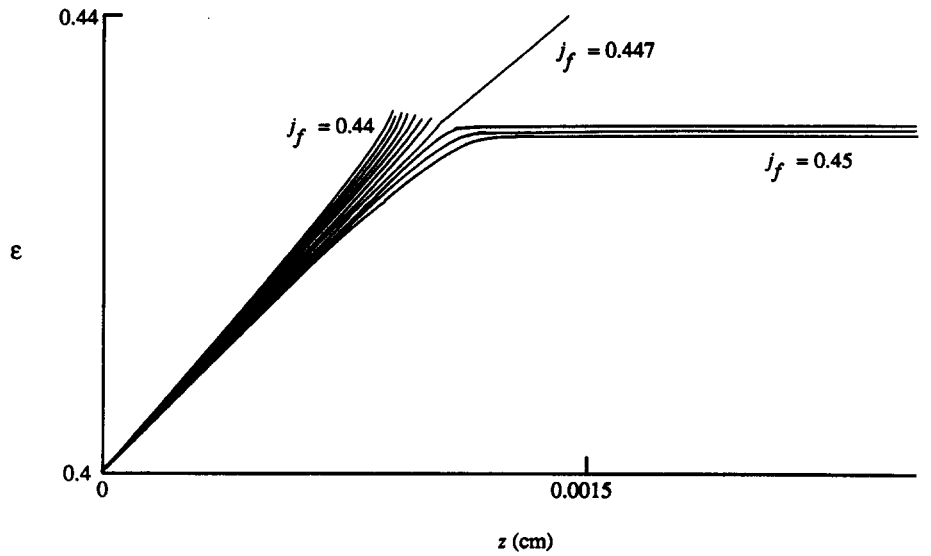


Figure 13. Numerical solutions to [32] for copper spheres ($d = 325\mu$m) in water, using $k = 0.43$, $j_s = 1.5$cm/s. The curves are for $j_f = 0.44$ to 0.45 step 0.001 cm/s. Only $j_f = 0.447$ allows smooth passage through point "$b$". The curves for $j_f < 0.447$ stop because $d\epsilon/dz$ becomes large.

The above method may be used to predict the entire dependence of the wave speed on the applied fluid flux, once some assumption is made about the parameter "$k$". Fortunately, however, it is not necessary to solve [32] and search for solutions passing through $b$ since an approximate analytical solution is possible if [35] is invoked.

At the critical condition the denominator of [32] is zero and, therefore, from [35] and [1]:

$$j_s = (1 - \varepsilon_b)^{3/2} U, \qquad [36]$$

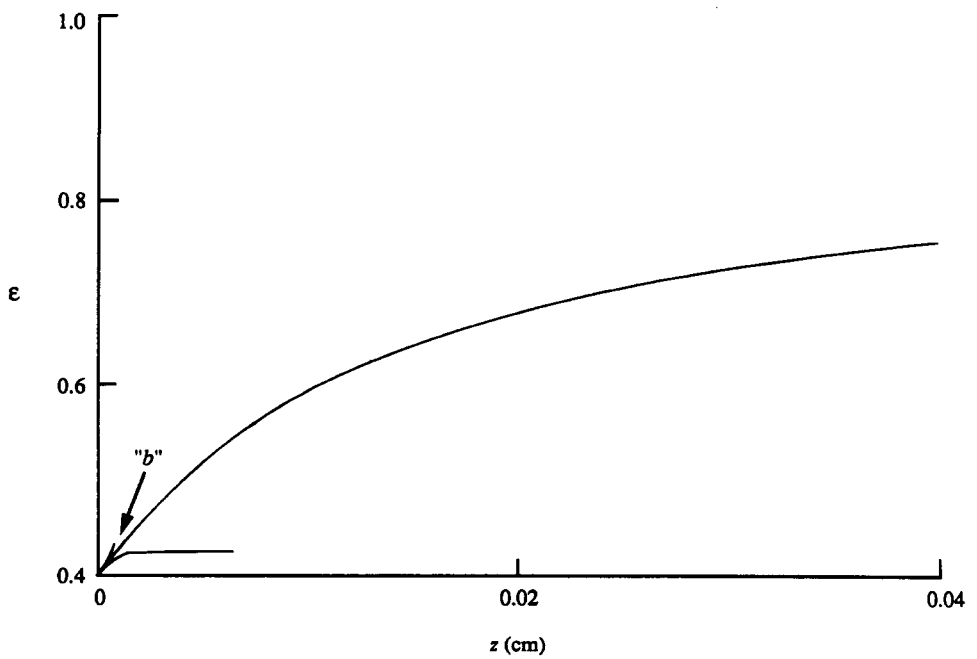


Figure 14. The solution in figure 13 developed to large values of $z$. The bifurcation point "$b$" occurs close to the start (top) of the wave.

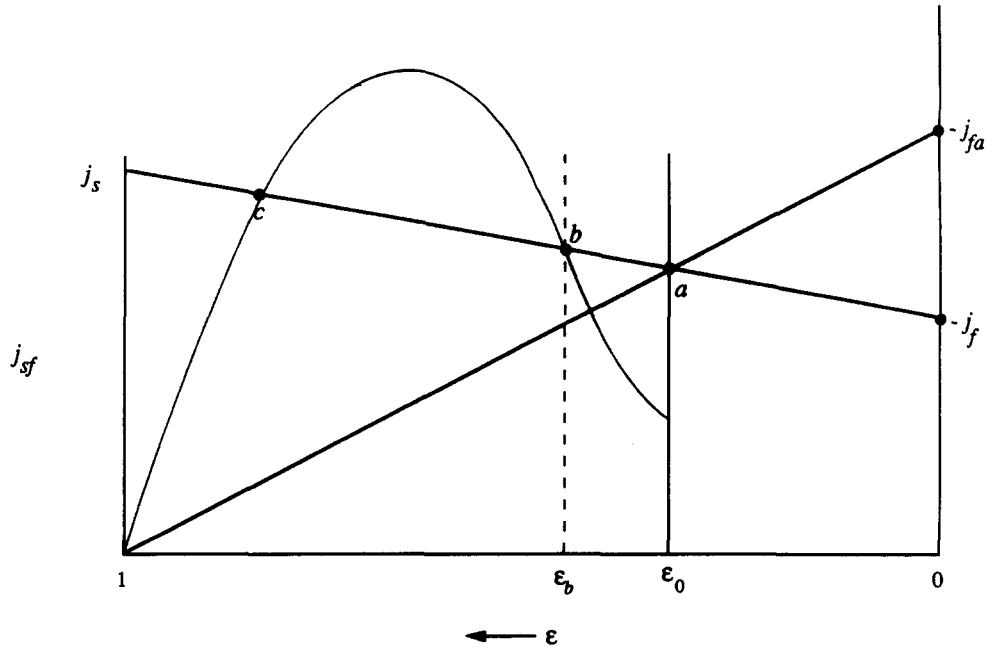


Figure 15. Determination of the "critical" condition at point "$b$".

where $U$ is a "characteristic velocity",

$$U = \left[\frac{kgd(\rho_s - \rho_f)}{\rho_f}\right]^{1/2}. \quad [37]$$

Therefore $j_s$ can be determined as a function of $\varepsilon_b$. The wave speed follows from [26]:

$$-v_{dw} = \frac{j_s}{1-\varepsilon_0}. \quad [38]$$

From the geometry of figure 15,

$$\frac{(j_{sf})_a - j_s}{1-\varepsilon_0} = \frac{(j_{sf})_b - j_s}{1-\varepsilon_b}. \quad [39]$$

Now

$$(j_{sf})_b = v_\infty(1-\varepsilon_b)\varepsilon_b^n \quad [40]$$

and

$$(j_{sf})_a = -j_{fa}(1-\varepsilon_0). \quad [41]$$

Therefore, using [36], [40] and [41] in [39]:

$$-j_{fa} = -\frac{(\varepsilon_b - \varepsilon_0)}{1-\varepsilon_0}(1-\varepsilon_b)^{1/2}U + v_\infty \varepsilon_b^n. \quad [42]$$

Equations [38] and [42] may be made dimensionless and used to make a plot such as figure 16. The predictions for constant $k$ all lie below the continuity wave limit and continue to much higher values of $j_a/j_{mf}$ than are observed in practice. Continuation of the curves below $j_a/j_{mf} = 1$ is physically unrealistic, as are the results for large values of $k$ which correspond to intersections "$b$" in the "$c$" position.

This analysis may be extended to incorporate the additional terms, representing fluid inertia, on the LHS of [10]. When they are included, it turns out that the critical condition [35] is

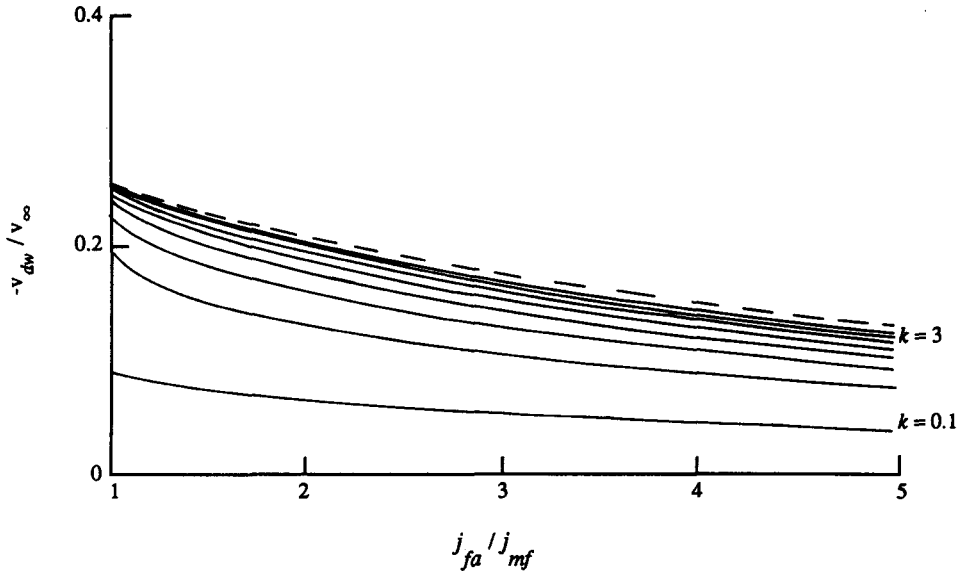


Figure 16. Prediction of decompression wave speed from "effective compressibility". 0.325 mm copper spheres in water: ——, $k = 0.1$ to 3 step 0.4; – – –, the continuity wave theory.

replaced by

$$(\rho_s + C\rho_f)\frac{j_s^2}{(1-\varepsilon)^3} + (\rho_f + C\rho_f)\frac{j_f^2}{\varepsilon^3} = kdg(\rho_s - \rho_f), \qquad [43]$$

which is to be solved simultaneously with the condition that point "$b$" lies on the equilibrium drift flux curve defined by [14]:

$$j_s\varepsilon - j_f(1-\varepsilon) = v_\infty(1-\varepsilon)\varepsilon^n. \qquad [44]$$

Using $\varepsilon$ as parameter, [43] and [44] may be solved for $j_s$ and $j_f$ which are used in [38] and [25] to obtain $v_{dw}$ and $j_{fa}$. Figure 17 compares this prediction, using $C = 0.5$, with the result obtained ignoring all terms involving $\rho_f$ on the LHS of [43], which gives predictions identical with [38] and [42]. For the case of 325 $\mu$m copper particles in water there is little difference between the two cases.

The predictions of this theory with a constant "compressibility coefficient", $k$, all give results extending to values of $j_{fa}/j_{mf}$ far beyond the range of the experimental data. A fit might then be sought by a suitable variation of $k$ with the parameters of the problem. For example, a dependence on solids concentration might be tried in the form

$$k = k_0\left(\frac{1-\varepsilon}{1-\varepsilon_0}\right)^b, \qquad [45]$$

which has the effect of making compressibility proportional to solids fraction raised to the power "$b$". The effect is not very encouraging if liquid inertia and added mass effects are excluded (figure 18). When these effects are included, it is possible to cover the data range for a given particle–fluid system (e.g. figure 19), but the magnitude of the index "$b$" that is required indicates a very strong dependency of compressibility on particle concentration.

While this theory might be used to fit decompression wave data, it must be regarded as tentative, in the absence of more direct measurements of the compressibility, if it exists. Moreover, the solutions contain two features, evident from figure 14, that challenge the basic assumption that the dispersion can be treated as a continuum:

- The slope $d\varepsilon/dz$ is discontinuous where the bottom of the solid stack of particles meets the top of the decompression wave. Individual particles physically bridge

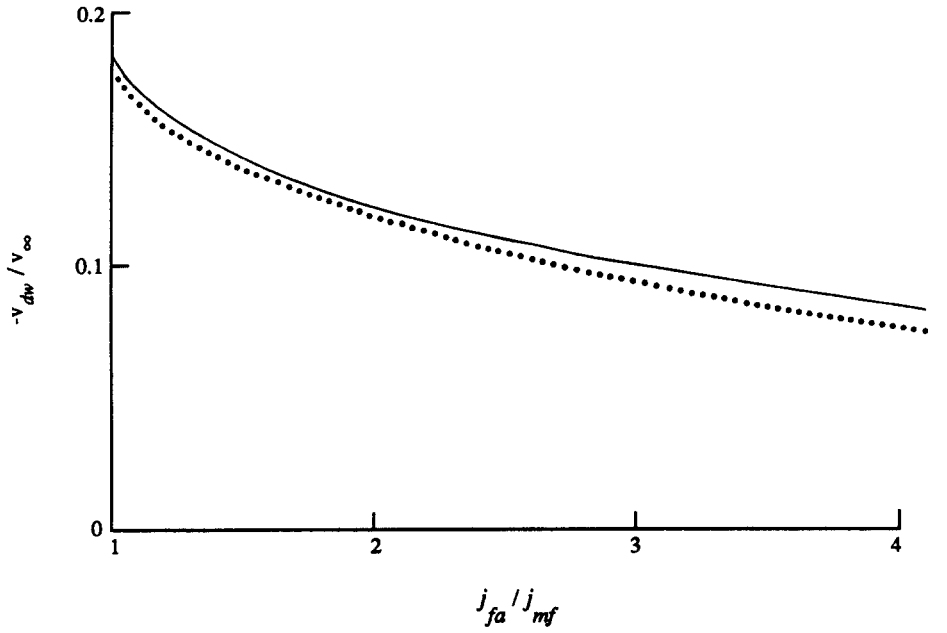


Figure 17. Effect of added mass and fluid inertia. 0.325mm copper spheres in water, $k = 0.43$: ——, particle inertia only; ···, included added mass and fluid inertia.

this discontinuity, yet their acceleration takes a step jump as their centers pass through it.

- The extent of the region of rapid acceleration is comparable with the particle size. For example, in figure 14 the void fraction changes from 0.4 to about 0.75 in a distance equal to the particle diameter, 0.0325 cm. The initial bifurcation point is reached when the particle has traveled about 3% of its own diameter! Perhaps a

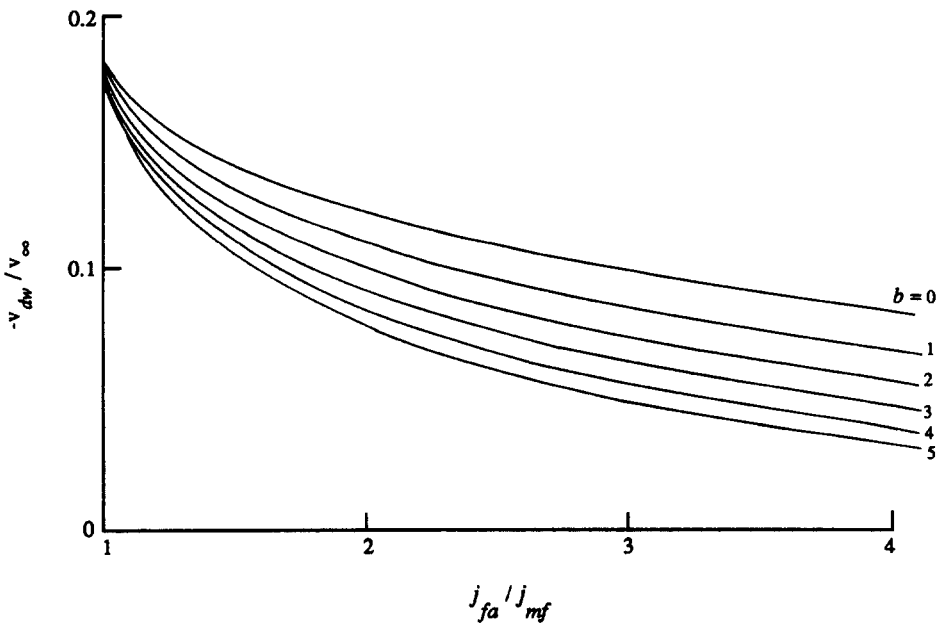


Figure 18. Compressibility described by [45]. 0.325mm copper spheres in water, $k = 0.43$; particle inertia only.

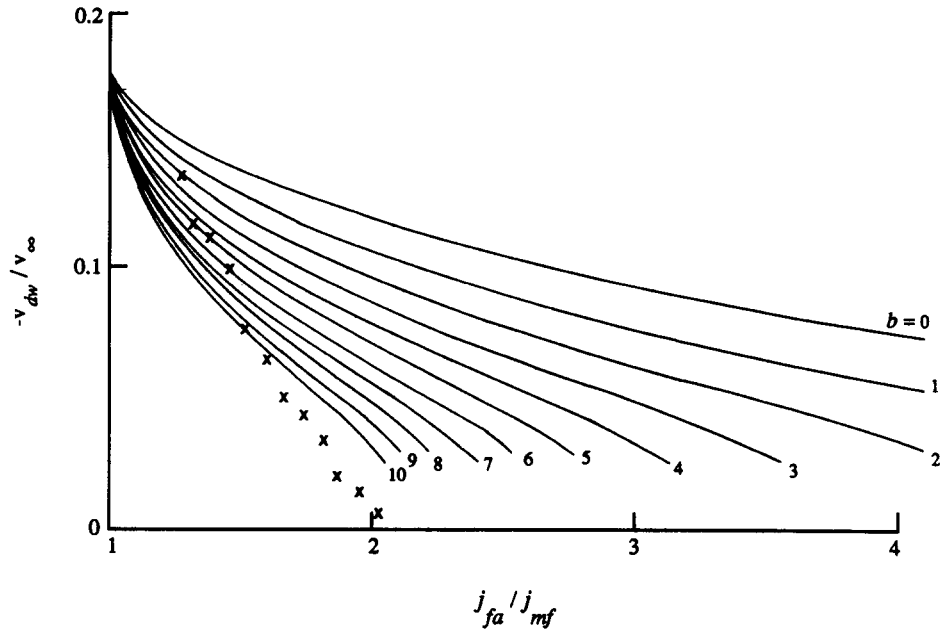


Figure 19. Compressibility described by [45]. 0.325mm copper spheres in water, $k = 0.43$. Added mass and fluid inertia included: ×, data of R. DiFelice (personal communication).

different approach is indicated when such large property changes occur on the scale of the individual particles.

### *3.6. Discretized model—hypothesis 2*

Indications that the void fraction changes significantly over the length of one particle within the decompression wave leads to basic questions about how the effective force on these particles is to be calculated. The approach described by Harvey (1991) is based on the idea that this force is determined by the relative velocity and the proximity of particles upstream and downstream of a given particle which is being "followed" by analysis. The effective void fraction for use in computing the mutual drag is some suitable average of the mean spacing of particles upstream and downstream from the particle under consideration.

Harvey (1991) followed the trajectories of a succession of typical particles using [10] without any additional terms and neglecting the fluid inertia term. Since only the particle velocity was of interest, the relative velocity was expressed in the equivalent form

$$v_f - v_s = \frac{j - v_s}{\varepsilon}, \qquad [46]$$

which is reminiscent of substitutions in terms of various relative velocities in the mutual diffusion of gas pairs (Bird *et al.* 1960). The equation to be solved is then

$$(\rho_s + C\rho_f)\frac{d^2z}{dt^2} = g(\rho_s - \rho_f) + \varepsilon_{\text{eff}}^{-4.7} C_{Ds}\frac{3}{4}\left(j - \frac{dz}{dt}\right)\left|j - \frac{dz}{dt}\right|, \qquad [47]$$

where $z$ is the coordinate along the trajectory of a given particle and $\varepsilon_{\text{eff}}$ is an "effective" void fraction. The approach is to label a series of equidistant particles, with separation $(\Delta z)_{pb}$ in the "packed bed" above the wave, and to follow the path of each one as it detaches and falls through the decompression wave (figure 20).

It seems reasonable to assume that $(\Delta z)_{pb}$ is of the order of a particle diameter, since this is the scale of the "range of influence" of a particle, and we may choose to write $(\Delta z)_{pb}$ as

$$(\Delta z)_{pb} = k_{sp} d. \qquad [48]$$

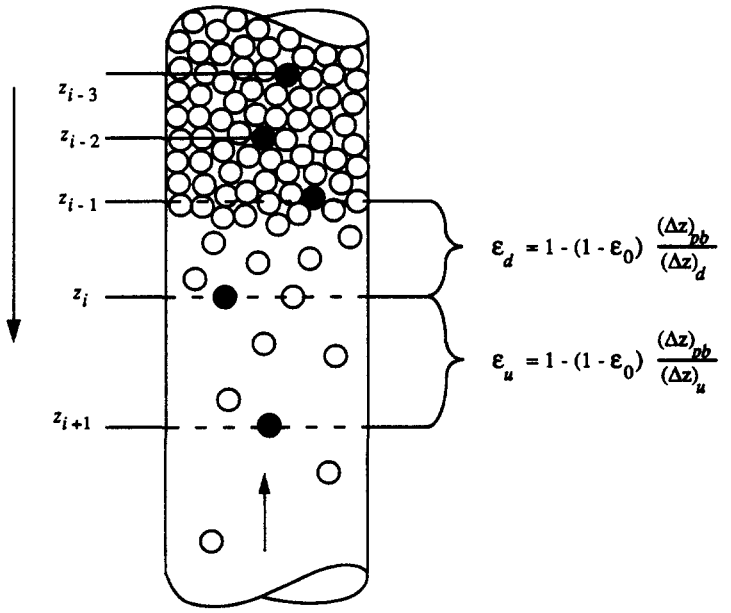


Figure 20. Nomenclature for the discretized model.

It is not clear what value should be assigned to $k_{sp}$. Visual observation suggests that particles fall off the bottom of the stack more or less one at a time rather than in large "clumps" or "clusters". We are therefore motivated to choose $k_{sp}$ based on the distance between two adjacent layers. In a close-packed bed, use of geometry leads to

$$k_{sp} = 0.8165. \qquad [49]$$

In all calculations made in this study, this close-packed value for $k_{sp}$ is used. However, in a real randomly packed stack of particles, it might be argued that a range of values for $k_{sp}$, of order 1, is plausible. In effect, $k_{sp}$ defines a "step size" for the spatial discretization of the void fraction profile and it is important to assess its influence on the predicted wave velocities. Figure 21 shows results obtained using the model outlined in Harvey (1991). Two cases are shown in the figure: a high $Re_\infty$ case ($Re_\infty = 3300$; 6 mm lead glass particles in water; $\rho_s = 2900\ kg/m^3$; $j_{fa}/j_{mf} = 1.1$); and a low $Re_\infty$ case ($Re_\infty = 29$; 425 $\mu$m lead glass particles in water; $\rho_s = 2900\ kg/m^3$; $j_{fa}/j_{mf} = 1.1$).

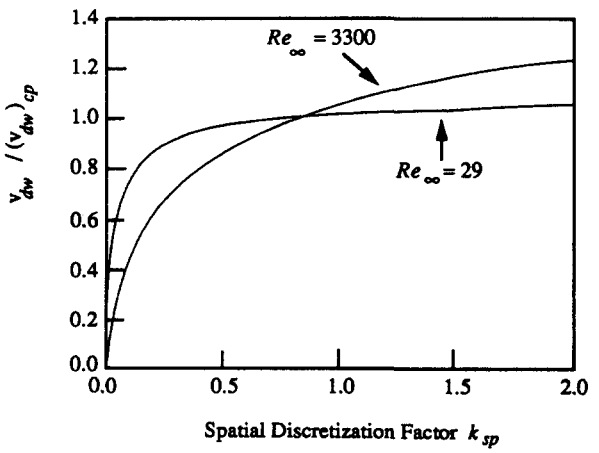


Figure 21. Influence of the spatial discretization factor $k_{sp}$ on predicted wave velocities.

For comparison purposes, the wave velocities $v_{dw}$ are scaled by $(v_{dw})_{cp}$, the latter being the wave velocity obtained for $k_{sp}$ set to the close-packed value.

The figure shows clearly that for larger $\mathrm{Re}_\infty$ the predicted wave velocities are more sensitive to variations in the spatial discretization factor $k_{sp}$ than for lower $\mathrm{Re}_\infty$ values. Indeed, unless $k_{sp}$ is unreasonably small, the predicted wave velocities for the small $\mathrm{Re}_\infty$ case do not vary much with $k_{sp}$. Figure 21 shows that within reasonable limits, variation of $k_{sp}$ influences the predicted wave velocities by no more than 10–20%, which is adequate for the first-order type analysis made. We will retain for the remainder of this paper the close packed value $k_{sp} = 0.8165$. In a more comprehensive study it might be possible to optimize the choice of $k_{sp}$.

Figure 21 also shows that, as $k_{sp} \to 0$, the predicted wave velocities drop rapidly towards a "stationary wave", corresponding to a situation with no movement of particles at the bottom of the stack. This limit corresponds to the continuum description of the decompression wave experiment. As expected, the wave velocity tends towards zero since a continuum description is unable to predict decompression wave behavior unless extra "force components" are introduced.

Referring to figure 20, we have the following kinematic description of the motion:

- $z_i$ refers to the $z$ location of the characteristic particle "$i$".
- $(\Delta z_u)_i$ and $(\Delta z_d)_i$ refer to the distances between the characteristic location "$i$" and the adjacent characteristic locations with indexes "$i+1$" and "$i-1$", respectively. Subscripts "$u$" and "$d$" refer to the upstream and downstream conditions, so that we have

$$(\Delta z_u)_i = z_{i+1} - z_i \qquad [50]$$

and

$$(\Delta z_d)_i = z_i - z_{i-1}. \qquad [51]$$

If we know the void fraction $\varepsilon_0$ corresponding to packed bed conditions, we may evaluate the equivalent upstream and downstream void fractions as follows:

$$(\varepsilon_u)_i = 1 - (1 - \varepsilon_0)\frac{k_{sp} d}{(\Delta z_u)_i} \qquad [52]$$

and

$$(\varepsilon_d)_i = 1 - (1 - \varepsilon_0)\frac{k_{sp} d}{(\Delta z_d)_i}. \qquad [53]$$

The key question now is how the net force on the particle is to be computed from $(\varepsilon_u)_i$ and $(\varepsilon_d)_i$.

Harvey (1991) tried various approaches. One was to assume an effective void fraction given by a linear combination

$$\varepsilon_{\mathrm{eff}} = \beta \varepsilon_u + (1 - \beta)\varepsilon_d. \qquad [54]$$

Comparing predictions with his data for 6 mm lead glass particles fluidized with water, Harvey found that $\beta = 0.5$ only gave reasonable results at the higher wave speeds. A much lower value of $\beta$ was needed to predict the condition where the wave speed drops to zero (figure 22).

Using arguments about the mechanics of drag in an assembly, Harvey argued for a non-linear averaging procedure of the form

$$\varepsilon_{\mathrm{eff}}^m = \beta \varepsilon_u^m + (1 - \beta)\varepsilon_d^m. \qquad [55]$$

Good results were obtained with $\beta = 0.5$ and $m = -4.7$ (figures 23 and 24), which corresponds to linear averaging of the upstream and downstream values of the factor involving $\varepsilon$ in [47].

This approach may seem more satisfying than the previous one, in which an effective compressibility was assumed, in that no additional terms were hypothesized in [47]. There also appears to be minimal empiricism in [55], which can be justified mechanistically. However, the

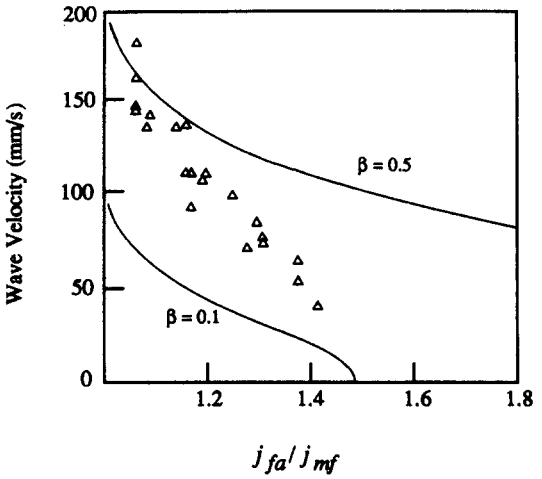


Figure 22. Attempts to fit data with two values of $\beta$ in [54]. 6mm lead glass particles in water.

averaging recipe is not unrelated to the "additional terms" hypotheses, as we shall see in the next section.

A typical void fraction profile predicted from this theory is compared with the result, for the same initial conditions (a step jump from $\varepsilon = \varepsilon_0$ to $\varepsilon = 1$ at $z = 500$ mm), derived from continuity wave theory in figure 25. The form of the leading edge of the decompression wave is identical in both cases. However, the top of the wave propagates into the packed bed at a slower speed when the discretized model is used. Just below the packed bed there is a rapid transition to a uniform void fraction, corresponding to point "$c$" in figure 12, which extends over to join the back end of the "expansion" wave.

### *3.7. Force proportional to $d^2\varepsilon/dz^2$—hypothesis 3*

By expanding the foregoing "averaging" method in a Taylor series, it can be related to hypotheses that represent an influence of void fraction gradients on the forces acting on the particles.

Consider, for example, particles in or near the stack, a distance $k_{pb}d$ apart. Focusing on one particle, the upstream and downstream void fractions will be computed at a spacing $\Delta = k_{pb}d/2$ from that particle and the finite-difference equivalents of the derivatives are

$$\frac{\partial \varepsilon}{\partial z} \simeq \frac{\varepsilon_u - \varepsilon_d}{2\Delta} \qquad [56]$$

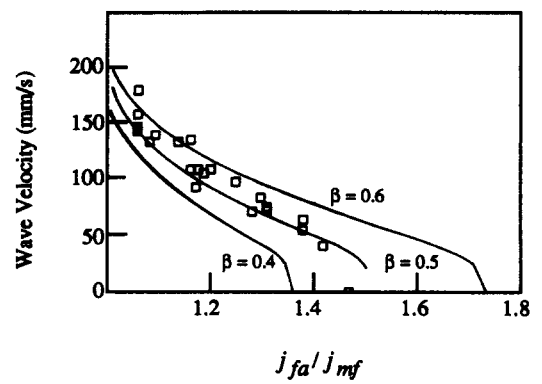


Figure 23. Use of various values of $\beta$ in [55]. 6mm lead glass particles in water.

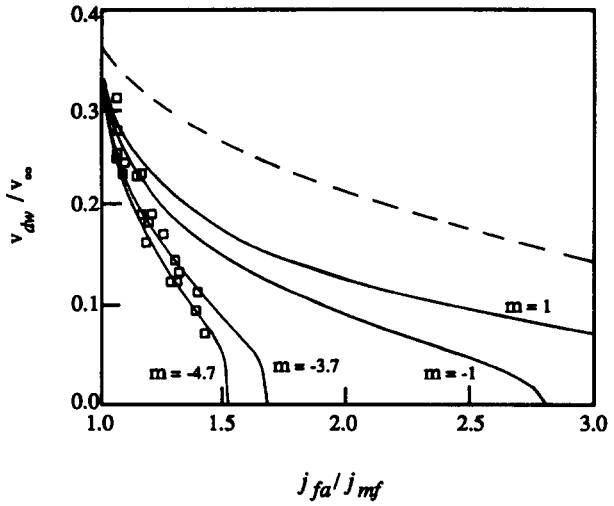


Figure 24. Effect of averaging the exponent $m$ on predicted wave velocities. 6mm lead glass particles in water: ---, continuity wave theory.

and

$$\frac{\partial^2 \varepsilon}{\partial z^2} \simeq \frac{\varepsilon_u + \varepsilon_d - 2\varepsilon}{\Delta^2}. \qquad [57]$$

Using these expressions in [54], we obtain

$$\varepsilon_{\text{eff}} = \beta\varepsilon_u + (1-\beta)\varepsilon_d = \varepsilon + (2\beta - 1)\Delta \frac{\partial \varepsilon}{\partial z} + \frac{\Delta^2}{2}\frac{\partial^2 \varepsilon}{\partial z^2}; \qquad [58]$$

while, if [55] is used and terms in $(\partial\varepsilon/\partial z)^2$ are neglected, the result is

$$\varepsilon_{\text{eff}}^m = \varepsilon^m \left[ 1 + (2\beta - 1)m \frac{\Delta}{\varepsilon}\frac{\partial \varepsilon}{\partial z} + \frac{m\Delta^2}{2\varepsilon}\frac{\partial^2 \varepsilon}{\partial z^2} + \cdots \right]. \qquad [59]$$

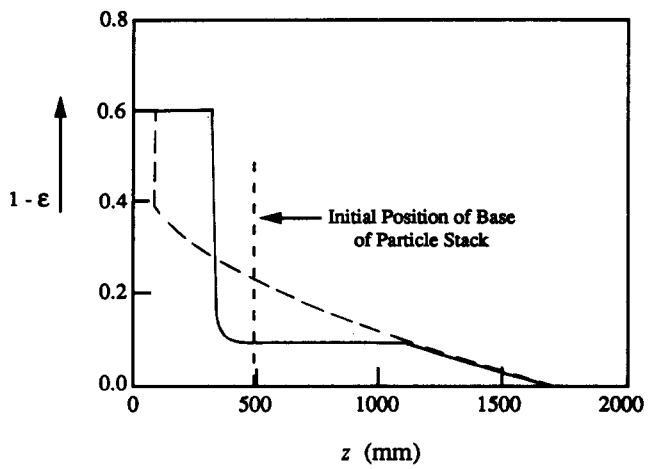


Figure 25. Decompression wave: solid concentration profiles. ---, Continuity wave theory; ——, discretized model. 6mm lead glass particles in water; initial stack size: 100 layers of particles; situation after 2.4s.

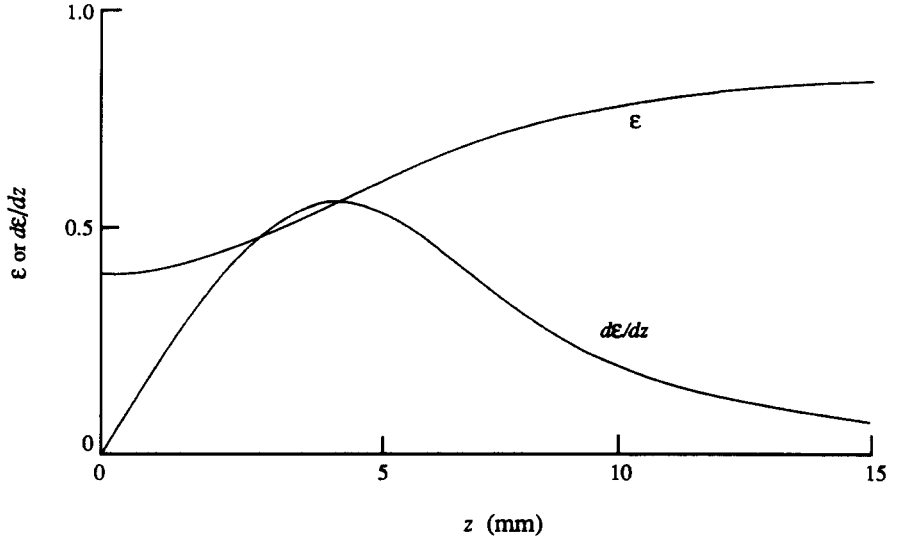


Figure 26. Void fraction profile for decompression wave derived from [62]. 6mm lead glass in water. $j_f = -80$mm/s, $j_s = 3.9$mm/s, $j_{fa}/j_{mf} = 1.49$, $v_{dw} = 60$mm/s, $k_2 = 1$.

Using the values found previously ($m = -4.7$, $\beta = 1/2$), [59] reduces to

$$\varepsilon_{\text{eff}}^{-4.7} = \varepsilon^{-4.7}\left[1 - \frac{4.7\Delta^2}{2\varepsilon}\frac{\partial^2\varepsilon}{\partial z^2} + \cdots\right]. \qquad [60]$$

In or near the packed bed, $\Delta \sim k_{pb}d/2 \sim 0.8165d/2$ and [60] becomes

$$\varepsilon_{\text{eff}}^{-4.7} = \varepsilon^{-4.7}\left[1 - k_2 d^2\frac{\partial^2\varepsilon}{\partial z^2}\right] \qquad [61]$$

with $k_2 \simeq 0.4$.

We may now use [61] to substitute in the final term in [47] and return to the Eulerian form [10], written as

$$(\rho_s + C\rho_f)v_s\frac{\mathrm{d}v_s}{\mathrm{d}z} - (\rho_f + C\rho_f)v_f\frac{\mathrm{d}v_f}{\mathrm{d}z} = g(\rho_s - \rho_f) + \frac{3}{4}\varepsilon^{-4.7}C_{Ds}\rho_f(j - v_s)|j - v_s|\left(1 - k_2 d^2\frac{\mathrm{d}^2\varepsilon}{\mathrm{d}z^2}\right). \qquad [62]$$

Substituting for $v_s$ and $v_f$ from [1] and [2], we obtain a differential equation which can be solved for $\varepsilon$. The approach is to assume values of $j_s$ and $j_f$ in the frame of reference in which the wave is at rest and to integrate forward in $z$, starting with $\varepsilon = \varepsilon_0$, $\mathrm{d}\varepsilon/\mathrm{d}z = 0$. For sets of unique combinations of $j_s$ and $j_f$, the solution tends asymptotically to the equilibrium state "$c$" in figure 12. Otherwise, it veers off on an excursion to unrealistically high or low extremes of $\varepsilon$. The situation qualitatively resembles behavior near the bifurcation point shown in figure 13. Most of the change in $\varepsilon$ again occurs over a few particle diameters, but there is no discontinuity in the slope of the void fraction profile at the top of the wave (figure 26).

A set of predicted wave speeds for different values of $k_2$, neglecting both added mass and liquid inertia effects, is shown in figure 27 for one of the systems studied by Harvey (1991). When added mass and liquid inertia are added, the fit is slightly better, showing a greater reduction of wave speed as the fluid flux is increased (figure 28).

### *3.8. Geometrical averaging—hypothesis 4*

Up to now we have accepted [1] and [2] as valid, even when the particle concentration changes significantly on the scale of the particles. As pointed out by Singh & Joseph (1991), this is not true. It is essentially the number density, and not the volume or area fraction occupied by particles, which should appear in the continuity equation. Let the particles each have an internal origin at a specified

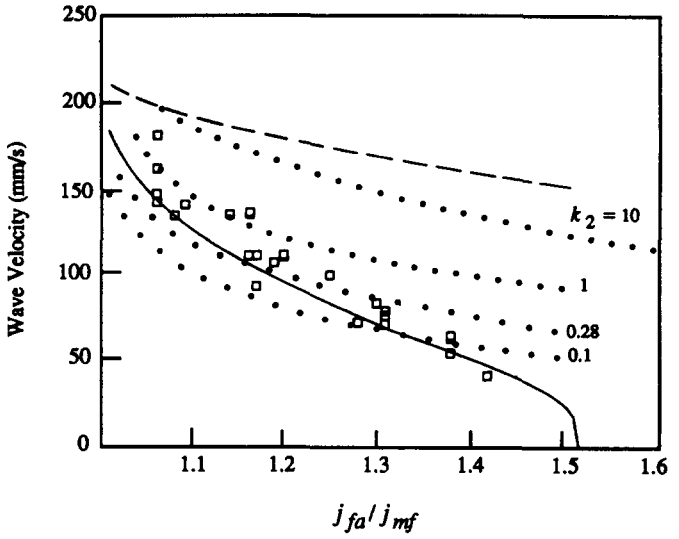


Figure 27. Data for 6mm lead glass particles in water, compared with three theories. ---, Continuity wave theory; ···, [62] with various values of $k_2$ but neglecting added mass and fluid inertia; ——, discretized model.

internal point (such as the centroid) and internal coordinates $z'$ relative to this point. The true conservation law that replaces [1] when particles move in the $z$-direction is

$$J_s = v_s n, \qquad [63]$$

where $J_s$ is the "number flux" and $n[z]$ is the number of centroids per unit volume (i.e. there are $n\,dz$ per unit cross-sectional area in the interval $dz$). $J_s$ is constant in steady flow. From straightforward geometry, sketched in figure 29, the area fraction of particles at $z$ is

$$\alpha[z] = \int_{z'_a}^{z'_b} A[z']n[z - z']\,dz', \qquad [64]$$

where $A[z']$ is the area of cross-section of a particle at the internal coordinate $z'$. $z'_a$ and $z'_b$ are the extreme values of $z'$ at the ends of the particle. For the present purposes we assume that the

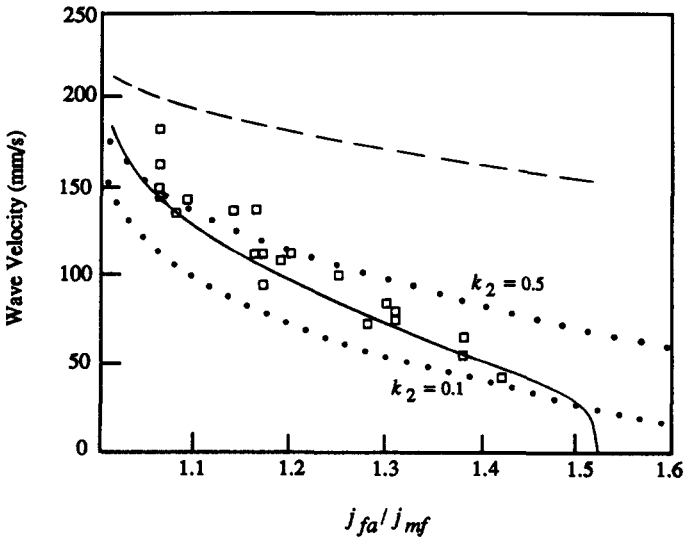


Figure 28. Same as figure 27 but with all terms used in [62].

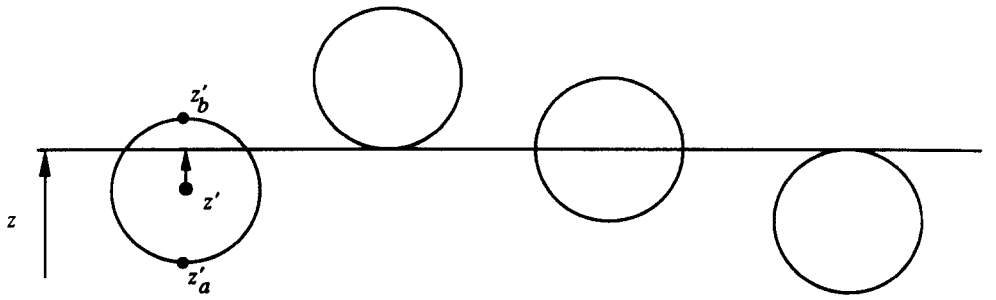


Figure 29. Derivation of area fraction from number density.

particles are identical and are all oriented the same way (or are spherical). Equation [64] represents a convolution between $\alpha$ and $n$. In general, we cannot replace $\alpha$ by $nV_p$, where $V_p$ is the volume of one particle, unless $n$ is a constant.

If $n$ is expanded as a Taylor series about the point $z$, [64] may be written as

$$\alpha[z] = nV_p - \frac{\mathrm{d}n}{\mathrm{d}z}\int_{z'_a}^{z'_b} A'z'\,\mathrm{d}z' + \frac{\mathrm{d}^2n}{\mathrm{d}z^2}\int_{z'_a}^{z'_b} A'\frac{z'^2}{2}\mathrm{d}z' + \text{etc.} \qquad [65]$$

By making the natural choice that the origin of $z'$ is at the geometrical centroid of the particle, the term in $\mathrm{d}n/\mathrm{d}z$ may be removed from [65]. Furthermore, we may define a "void fraction" based on the number density,

$$(1 - \varepsilon_n) = nV_p, \qquad [66]$$

so that the true continuity equation, obtained by multiplying [63] by $V_p$, is

$$j_s = V_p J_s = v_s(1 - \varepsilon_n), \qquad [67]$$

while the "void fraction" based on the "area fraction occupied by particles at $z$" is defined as

$$\varepsilon_a = 1 - \alpha. \qquad [68]$$

Then [65] may be reexpressed as

$$\varepsilon_a = \varepsilon_n + \frac{\partial^2\varepsilon_n}{\partial z^2}\frac{1}{V_p}\int_{z'_a}^{z'_b} A'\frac{z'^2}{2}\mathrm{d}z' + \text{etc.} \qquad [69]$$

The coefficient multiplying $\partial^2\varepsilon_n/\partial z^2$ in [69] is a purely geometrical property of the particles. For spheres it turns out to be $d^2/40$ and [64] becomes, ignoring higher order terms,

$$\varepsilon_a = \varepsilon_n + \frac{d^2}{40}\frac{\partial^2\varepsilon_n}{\partial z^2}. \qquad [70]$$

Now, when we solve for the particle motion using [3], we may use [67] to eliminate $v_s$ on the LHS and obtain a differential equation for $\varepsilon_n$. However, the key questions now are which $\varepsilon$ is to be used in constitutive laws such as [5] and [6] and how $v_f$ is to be computed for use in these equations (if indeed they can still be used).

One assumption, which is relatively simple to use, is based on substituting [46] in [10], arguing that $j$ is constant throughout the flow and can be computed "somewhere", and claiming that the factor $\varepsilon^{-4.7}$ should involve the area fraction $\varepsilon_a$. The solution variable is $\varepsilon_n$, so $\varepsilon^{-4.7}$ should be replaced by

$$\varepsilon_a^{-4.7} = \left(\varepsilon_n + \frac{d^2}{40}\frac{\partial^2\varepsilon_n}{\partial z^2}\right)^{-4.7} \simeq \varepsilon_n^{-4.7}\left[1 - \frac{4.7d^2}{40\varepsilon_n}\frac{\partial^2\varepsilon_n}{\partial z^2}\right]. \qquad [71]$$

The upshot of making the approximation in [71] is entirely equivalent to what was done in [61], except that we now have a prediction of the value of $k_2$:

$$k_2 = \frac{4.7}{40\varepsilon_n}. \qquad [72]$$

At the top of the wave, where $\varepsilon_n$ changes very rapidly and the wave speed appears to be controlled, $\varepsilon_n \sim \varepsilon_0 \sim 0.4$ and [72] yields

$$k_2 \sim 0.29, \qquad [73]$$

which seems a reasonable choice in figure 27, but, as we shall see, does not necessarily work for all fluid–particle combinations.

Of course, [71] represents an approximation and it might be more satisfactory, when $\varepsilon$ changes rapidly with $z$, to use the entire convolution in [64], as was done by Singh & Joseph (1991) in an investigation of wave propagation in a two-dimensional (planar) fluidized bed but is difficult to incorporate into the numerical schemes used here. An intermediate approach is not to use the approximation in [71] but to use [70] to substitute directly for $\varepsilon$ in the drag law. There are still some interesting questions about which of the $\varepsilon$s in the original theory are to be replaced by $\varepsilon_a$. For example, if it is only the $\varepsilon$ in [5] that is to be modified we can identify $\varepsilon$ in [1] and [2] as $\varepsilon_n$ and express [10] as

$$\left[(\rho_s + C\rho_f)\frac{j_s^2}{(1-\varepsilon)^3} + (\rho_f + C\rho_f)\frac{j_f^2}{\varepsilon^3}\right]\frac{\mathrm{d}\varepsilon}{\mathrm{d}z}$$

$$= g(\rho_s - \rho_f) + \frac{3}{4}C_{Ds}\rho_f \frac{(v_f - v_s)|v_f - v_s|}{d}\left(\varepsilon + \frac{d^2}{40}\frac{\mathrm{d}^2\varepsilon}{\mathrm{d}z^2}\right)^{-2.7}. \qquad [74]$$

The method of solution is now to solve [74] for $\mathrm{d}^2\varepsilon/\mathrm{d}z^2$ and proceed to solve for $\varepsilon$ as a function of $z$, starting from $z = 0$, $\mathrm{d}\varepsilon/\mathrm{d}z = 0$, $\varepsilon = \varepsilon_0$. Some results of this process are shown in figure 30 and show the emergence of an interesting "cliff" at $j_{fa}/j_{mf} \simeq 1.45$, for which there is some empirical support.

An alternative approach might be based on a modification of the final term in [47], so that the last term in [74] would be replaced by

$$\frac{3}{4}C_{Ds}\rho_f \frac{(j - v_s)|j - v_s|}{d}\left(\varepsilon + \frac{d^2}{40}\frac{\mathrm{d}^2\varepsilon}{\mathrm{d}z^2}\right)^{-4.7}. \qquad [75]$$

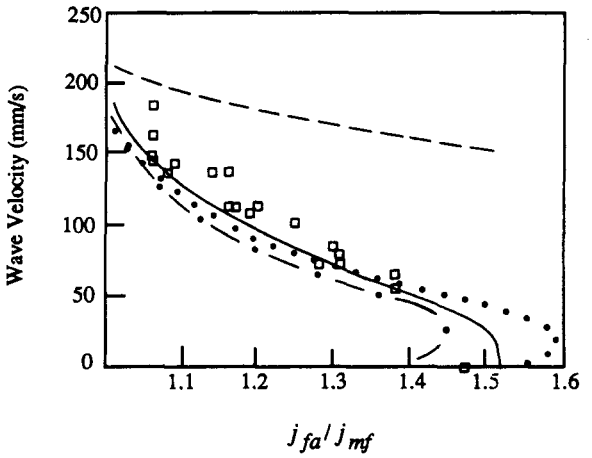


Figure 30. Data for 6mm lead glass particles in water compared with several theories. – – –, continuity wave theory; ——, discretized model; ···, [75]; —·—, [74].

The result of using this approach on 6 mm lead glass particles fluidized with water is shown in figure 30, where the agreement with these data appears not to be influenced much by the choice of either method.

The appeal of this theory is that it is based on an "assertion", that the area fraction is the appropriate "$\varepsilon$" to use in the drag law, and does not contain adjustable empirical parameters. The key remaining question, which we will investigate in section 4, is how well it works for other fluid–particle systems.

### 3.9. The limit $v_{dw} \to 0$

A major feature of the experimental results is that, above a certain value of the applied flux, the particle stack remains static and there are no decompression waves. We denote this critical fluid flux by $(j_{fa})_0$; it corresponds to the situation where particles at the bottom of the stack are just supported against gravity by hydrodynamic forces. This situation could be simpler to analyze than wave propagation, since the dynamics of the particles are not involved.

If we neglect the fluid inertia terms in [10], what remains is merely the balance between the "drag" term and the submerged weight of the particles. For Harvey's discretized model this balance may be expressed as

$$g(\rho_s - \rho_f) = \frac{3}{4} C_{Ds} \varepsilon_{\text{eff}}^{-4.7} \rho_f \frac{(j_{fa})_0^2}{d} \qquad [76]$$

with

$$\varepsilon_{\text{eff}}^{-4.7} = \frac{\varepsilon_0^{-4.7} + 1^{-4.7}}{2}. \qquad [77]$$

At incipient fluidization a similar balance yields

$$g(\rho_s - \rho_f) = \frac{3}{4} C_{Ds} \varepsilon_0^{-4.7} \rho_f \frac{j_{mf}^2}{d}. \qquad [78]$$

The drag coefficients in [76] and [78] depend on Re. For large Re, the $C_{Ds}$ are equal and we obtain

$$\frac{(j_{fa})_0}{j_{mf}} = \left( \frac{1 + \varepsilon_0^{-4.7}}{2} \right)^{-1/2} \qquad [79]$$

which, for $\varepsilon_0 = 0.4$, is equivalent to

$$\frac{(j_{fa})_0}{j_{mf}} = 1.405. \qquad [80]$$

On the other hand, at very low Re, where $C_D \propto 1/\text{Re}$, this ratio is close to 2.

If we adopt the geometrical averaging approach (hypothesis 4) and still neglect fluid inertia effects, the result is

$$\varepsilon_{\text{eff}} = \left( 1 - \frac{1 - \varepsilon_0}{2} \right) = \frac{1 + \varepsilon_0}{2} \approx 0.7 \qquad [81]$$

and we get, at high Re,

$$\frac{(j_{fa})_0}{j_{fm}} \simeq \left( \frac{0.7}{0.4} \right)^{4.7/2} = 3.725, \qquad [82]$$

which is too large.

It would appear to be more reasonable not to neglect the liquid inertia term in [10] and to increase the total hydrodynamic force by the amount $-(1 + C)\rho_f v_f \mathrm{d}v_f/\mathrm{d}z$, making reasonable estimates for the effective velocity and velocity gradient. This, of course, assumes that effects are additive, which is not necessarily so. (In a separate study, we have used boundary layer theory to estimate the drag on a particle in a converging fluid flow and found that at high Re there is a *decrease* in the drag force greater than the contribution from the "added mass" term involving $C$!) Since the mean fluid velocity outside the particle stack is $j_{fa}$ and the mean velocity inside is $j_{fa}/\varepsilon_0$, reasonable estimates

for the parameters are

$$v_f = \frac{j_{fa}}{2}\left(1 + \frac{1}{\varepsilon_0}\right) \quad [83]$$

and

$$\frac{dv_f}{dz} = -\frac{j_{fa}}{d}\left(\frac{1}{\varepsilon_0} - 1\right). \quad [84]$$

The result is a force (negative and therefore upward) on each (average) particle, per unit particle volume, of

$$-(1+C)\frac{\rho_f j_{fa}^2}{d}\frac{(\varepsilon_0+1)(1-\varepsilon_0)}{2\varepsilon_0^2}$$

which is equal to $-3.94\rho_f j_{fa}^2/d$ for $C = 1/2$ and $\varepsilon_0 = 0.4$.

An alternative estimate of this "accelerational" term may be obtained from the potential flow analysis of Wallis (1989) who showed that there is an effective pressure, or force per unit total area, on the surface of discontinuity between $\varepsilon = 1$ and $\varepsilon = \varepsilon_0$ equal to

$$-p_p = \frac{3}{4}\left(\frac{1-\varepsilon_0}{\varepsilon_0}\right)^2 \rho_f j_{fa}^2. \quad [85]$$

If this force is distributed over one layer of particles occupying an area fraction $(1-\varepsilon_0)$ with a number per unit area of $(1-\varepsilon)/(\pi d^2/4)$, the force per unit volume on these particles is

$$f_2 = -\frac{3}{4}\left(\frac{1-\varepsilon_0}{\varepsilon_0}\right)^2 \rho_f j_{fa}^2 \frac{\pi d^2}{4}\frac{1}{1-\varepsilon_0}\frac{6}{\pi d^3}$$
$$= -4.2\rho_f j_{fa}^2/d \quad (\text{if } \varepsilon_0 = 0.4), \quad [86]$$

which is close to the previous value and acting upwards (as indicated by the negative sign). This compares with the following "forces" calculated at high Re (i.e. $C_{Ds} \simeq 0.44$) by using the previous approaches:

*Discretized model,*

$$f_2 = -\frac{3}{4}(0.44)\left(\frac{0.4^{-4.7}+1}{2}\right)\frac{\rho_f j_{fa}^2}{d} = -12.4\frac{\rho_f j_{fa}^2}{d} \quad [87]$$

and

*geometrical averaging model,*

$$f_2 = -\frac{3}{4}(0.44)(0.7^{-4.7})\frac{\rho_f j_{fa}^2}{d} = -1.76\frac{\rho_f j_{fa}^2}{d}; \quad [88]$$

whereas, at incipient fluidization

$$f_2 = -\frac{3}{4}(0.44)0.4^{-4.7}\frac{\rho_f j_{mf}^2}{d} = -24.5\frac{\rho_f j_{mf}^2}{d}. \quad [89]$$

If we choose to add the "effects" in [86] and [87] and compare with [89], the result is

$$\frac{(j_{fa})_0}{j_{mf}} = \left(\frac{24.5}{12.4+4.2}\right)^{1/2} = 1.21, \quad [90]$$

whereas adding [86] to [88] leads to

$$\frac{(j_{fa})_0}{j_{mf}} = \left(\frac{24.5}{1.76+4.2}\right)^{1/2} = 2.03, \quad [91]$$

which is a large change from [82]. However, both [90] and [91] are within the range of observations.

Another "effect" that might be invoked is the "effective compressibility". The jump in void

fraction from $\varepsilon_0$ to 1 over a distance comparable to the particle diameter might be represented by a void fraction gradient of order

$$\frac{d\varepsilon}{dz} \sim \frac{1-\varepsilon_0}{d}, \qquad [92]$$

which, if used in [34], would reduce the "drag" component by the factor $[1-k(1-\varepsilon_0)]$ (suggesting that $k$ cannot be much larger than $\sim 1$). A similar argument predicts that the drag force on the particle layer at the top of a uniformly fluidized bed should be increased by a factor $1+k(1-\varepsilon)$. It is still an open question what effective void fraction should be used to compute the "force" which is to be modified by these factors. At low Re, because reversing the flow changes the sign of all velocities, surface stresses and pressure differences, the net drag force must clearly be the same whatever the sign of the voidage jump or gradient and it would appear that there can be no "effective compressibility" if the particles are at rest. The "discretized model" and "geometrical averaging" approach also lead to zero "effective compressibility" and both predict similar forces for particle layers on the top and bottom of a stationary particle stack through which fluid is flowing.

## 4. COMPARISONS WITH EXPERIMENTAL DATA

### *4.1. Force measurements*

Apart from measurements of the expansion characteristics of uniform fluidized beds, from which results resembling [12] can be obtained and used to justify recipes such as [5]–[9], there have been few direct measurements of the effect of neighboring particles on the hydrodynamic force exerted on one particle. This is particularly true of non-uniform assemblies in which there are gradients or jumps in the void fraction.

Rowe & Henwood (1961) measured the drag force on a particle in a close-packed assembly and found it to be 73 times as great as on a single particle immersed in the same fluid flux. They also measured the force on a single particle as a function of its distance upstream or downstream from an empty lattice point in the surface layer of an assembly. Their interpretation of their data appeared to support the "compressibility" hypothesis and was used by Wallis (1962) to estimate $k \simeq 1.4$. However, Harvey (1991) carefully examined the original data and concluded that there was no clear evidence for such a hypothesis.

Harvey (1991) used gravity to measure the force on particles in the upstream or downstream layer of a randomly packed assembly. To study the upstream layer he stacked glass particles ($\rho_s = 2900$ kg/m$^3$) of 1/16‴ dia at the top of a vertical column, as at the start of a decompression wave experiment. He then increased the water flux until a number of steel balls ($\rho_s = 7980$ kg/m$^3$) of the same diameter could be suspended and laid down as a surface layer on the outside of the assembly of glass particles. The water flux was then reduced in small steps and it was noted how many steel balls fell off at each stage. A histogram was then developed of the number of balls detaching as a function of $j_{fa}/j_{mf}$ and it was determined that, on the average, "rainoff" occurred at $(j_{fa}/j_{mf})_0 = 2.01$, with a standard deviation of 0.56.

To measure the force on the downstream layer of an assembly, Harvey established a stationary bed of copper particles ($\rho_s = 8600$ kg/m$^3$, $d = 1/16$″) at the bottom of a cylindrical column and settled a layer of aluminum particles ($\rho_s = 2800$ kg/m$^3$) of the same diameter on top of them. He observed that the lighter particles were first set in motion at an average value $(j_{fa}/j_{mf}) = 1.83$ with a standard deviation of 0.19. In other words, contrary to Rowe & Henwood's (1961) contention that the top layer of fluidized bed lifts off before the entire bed fluidizes, it took roughly 1.83 times the fluid flux to lift the surface particles than would be necessary to fluidize a bed consisting entirely of aluminum spheres of the same diameter. Harvey (1991) concluded that there was little direct evidence for a significant "compressibility" effect in a bed of stationary particles.

### *4.2. The limit $v_{dw} \to 0$*

It might be expected that careful measurements of the fluid flux at which particles are just able to detach from the bottom of the stack (i.e. $v_{dw}$ is very small) would provide good tests of the

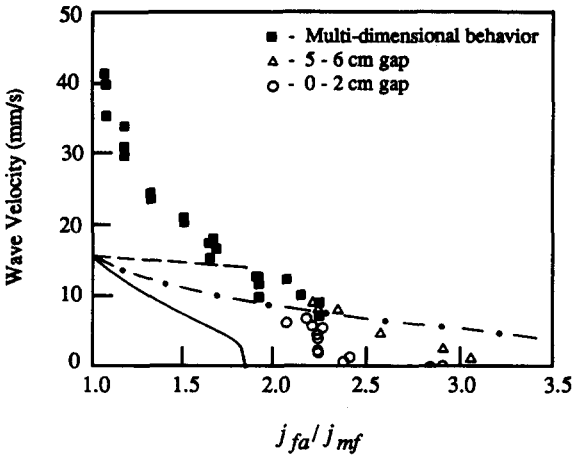


Figure 31. Decompression wave: 420 $\mu$m lead glass particles in water. A fluidized bed is established below the wave and the gap between the top of this bed and the bottom of the stack is varied ($\rho_s/\rho_f = 2.9$). ——, Discretized model; – – –, continuity wave theory; –·–, [74].

theories presented in section 3.9. Unfortunately, there are very few accurate data available in this region.

Buysman & Peersman (1967) studied the "rainoff" point and measured the pressure drop across the particle stack. They reported the ratio of this pressure drop to the buoyant weight of the particles. Using standard correlations for the pressure drop in packed beds it is possible to use their data to predict the ratio $(j_{fa})_0/j_{mf}$ For glass beads of 180–600 $\mu$m dia in air and $\epsilon = 0.4$, this ratio varies from 2.1 to 1.6, while for 600–1000 $\mu$m dia glass beads in water it ranges from 1.58 to 1.53, in agreement with our present results.

Buysman & Peersman (1967) also were able to compact the bed to values of $\epsilon$ as low as 0.32, introducing a new variable worthy of further study. They discuss the influence of particle–particle forces, particularly on compressed beds of small particles in air, where electrostatic and capillary forces may be significant. In our experiments on relatively large particles in water the mechanical interparticle forces are expected to dominate and we were careful not to use excessive pressure drop, vibration or other means that can compact the bed below $\varepsilon \sim 0.4$. Uncertainty about some of these effects could explain some scatter in the available data and deserves a more thorough future study.

Most of the evidence for the "rainoff" point is derived by extrapolating decompression wave data. The scatter in such results does not allow discrimination between the more successful theories. Moreover, there are some experimental problems in approaching the limit $v_{dw} \to 0$, which depends on how firmly the particle stack was packed (e.g. tapping the tube while the stack is compressed may make it compact more tightly), how constant the fluid flow is, the velocity profile and degree of turbulence in the oncoming flow and so on. At low wave velocities, propagation may be quite irregular, perhaps coming to rest for a time and recommencing as a chance vibration or other disturbance causes particles to be dislodged again. Such erratic behavior might be inherent if predictions like those displayed in figure 30 are qualitatively correct, with the wave velocity being multi-valued or insensitive to $j_{fa}$ near the limit of interest. Particular difficulty occurs with small particles which may either not fall at all or fall off as multi-particle "chunks", leading to a multi-dimensional flow pattern.

In an attempt to promote one-dimensional behavior in a system of small (420 $\mu$m dia) glass balls in water, experiments were run with a fluidized bed established just beneath the particle stack (figure 31). The wave speed was observed to depend on the size of the gap between the top of the fluidized bed and the bottom of the particle stack (both of which propagate upwards during the experiment with the "gap" in which the decompression wave occurs continuously narrowing). The limiting value, $(j_{fa})_0$, depends significantly on the gap size.

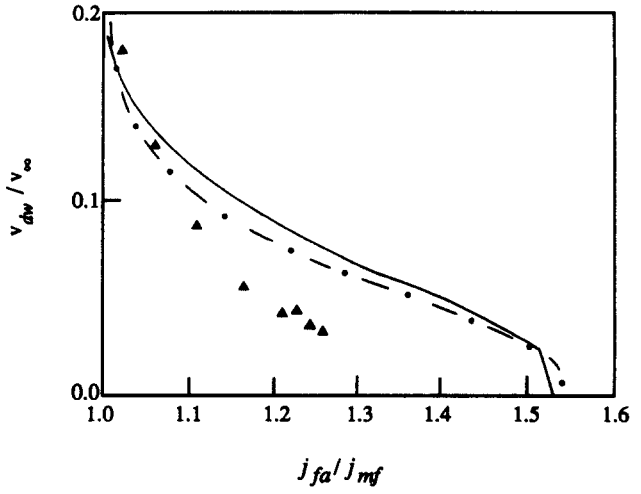


Figure 32. Decompression wave speed for 2.4 mm lead shot in water, $Re_\infty = 2250$. ——, Discretized model; —·—, [74]; ▲, data of DiFelice (personal communication).

Qualitatively, $(j_{fa})_0/j_{mf}$ is generally lower at higher Re (figure 5), as all the theories predict, and the limit predicted in [80] appears reasonable. Equation [90] is probably too low and [91] too high, but the data are neither extensive enough nor precise enough to lead to unequivocal conclusions.

### 4.3. *Decompression wave velocities*

Comparisons that were presented in section 3 appeared to show that data were best represented by the discretized model, a force proportional to $\partial^2\varepsilon/\partial z^2$ or by the geometrical averaging approach, all of which are approximately equivalent when $j_{fa}$ is close to $j_{mf}$. These approaches will now be compared with further data, the major parameters being the particle diameter and the solid/fluid density ratio.

Figure 32 presents results for lead shot fluidized by water ($\rho_s/\rho_f = 11$, $d = 2.4$ mm). Both the discretized model and the $\partial^2\varepsilon/\partial z^2$ effect theory, using [74], are close to the data near $j_{fa}/j_{mf} = 1$ but wave velocities are overpredicted as $j_{fa}$ is increased.

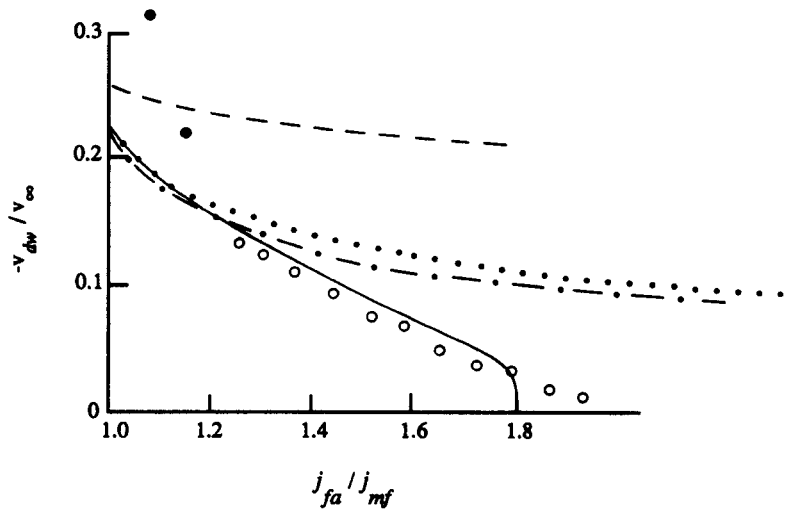


Figure 33. 0.325 mm copper spheres in water. ——, Discretized model; —·—, [74]; ···, [62] and [73]; – – –, continuity wave theory. From DiFelice (personal communication): ○, one-dimensional wave; ●, three-dimensional wave.

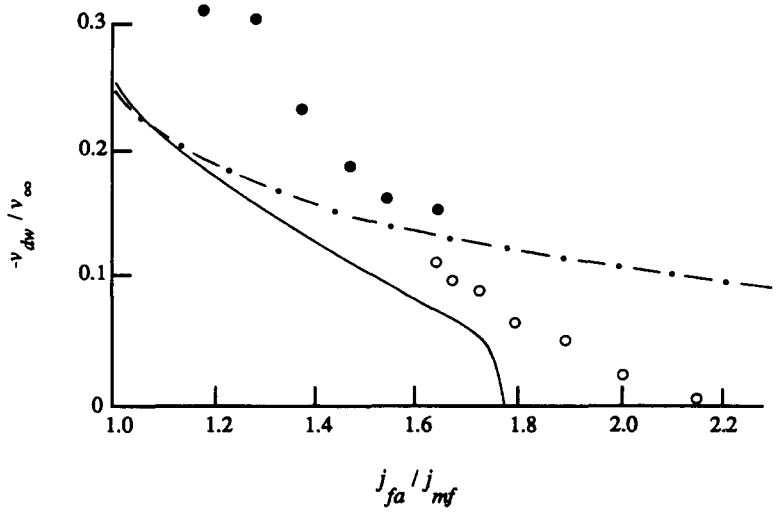


Figure 34. 0.65 mm copper spheres in water. ——, Discretized model; —·—, [74]. From DiFelice (personal communication): ○, one-dimensional wave; ●, three-dimensional wave.

Figure 33 shows a similar comparison with data for copper spheres fluidized with water ($\rho_s/\rho_f = 8.9$, $d = 0.325$ mm). The discretized model is close to the data but the geometrical averaging approach, using [74], or the $\partial^2\varepsilon/\partial z^2$ effect theory, with $k_2 = 0.29$, significantly overpredict the data, as in figure 32.

Figure 34 presents results for lead glass spheres in water ($\rho_s/\rho_f = 2.9$, $d = 0.65$ mm). Though the points appear to form a continuous curve, many of the data correspond to three-dimensional waves. Neither of the theories is particularly accurate. Our results for 1 and 2 mm lead glass particles are similar. As the diameter is further decreased, these trends continue (figure 31).

Results for the lowest density ratio ($\rho_s/\rho_f = 2.5$) and highest Re ($Re_\infty = 4500$, $(Re_s)_{mf} = 490$) that we have tested are presented in figure 35. As in the similar comparisons in figure 30, the prediction using [74] appears to present a lower bound to the data, but could be made to pass optimally through the points by decreasing $j_{mf}$ by a few percent ($\sim 5\%$), which is within the precision of both measurement and theory for the minimum fluidization flux.

Since smaller particles and low density ratios (low Re) lead to some of the biggest deviations between theory and experiment, we reinvestigated the influence of the "averaging exponent", $m$, in [55]. For 425 $\mu$m lead glass particles in water (figure 36) no clear resolution is achieved by choosing any particular value of $m$.

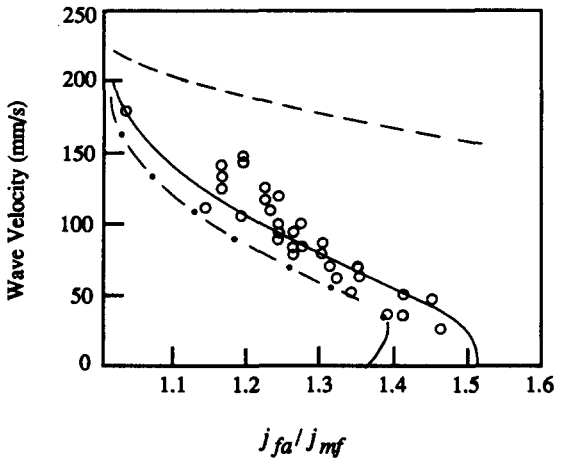


Figure 35. 8 mm soda glass particles ($\rho_s = 2500$ kg/m$^3$). ---, Continuity wave theory; ——, discretized model; —·—, [74]. $Re_\infty = 4500$.

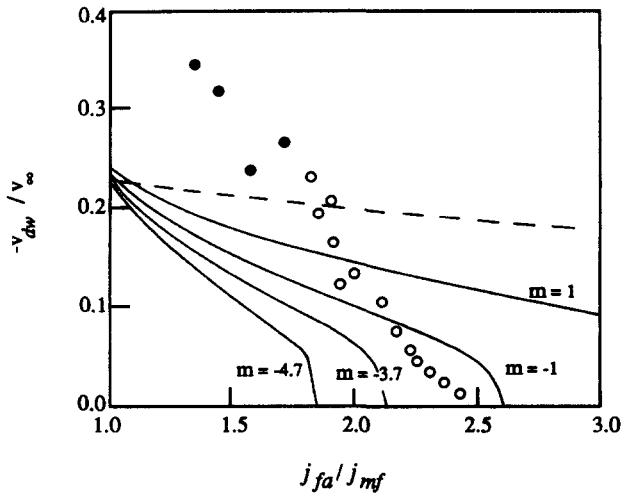


Figure 36. Effect of averaging exponent $m$ on predicted wave velocities: 425$\mu$m lead glass particles. ● Three-dimensional data; ○, one-dimensional data; ——, continuity wave theory.

## 5. DISCUSSION AND CONCLUSIONS

Decompression wave data provide a test of constitutive equations for dispersed particle systems. It is impossible to predict these phenomena from current continuum theories that use interphase drag forces based solely on relative velocity and local void fraction.

The most successful hypotheses for predicting the velocity of these waves, as long as they remain one-dimensional, are:

- A "discretized" model, based on non-linear averaging of upstream and downstream void fraction at some specified spacing scaled by the particle size (Harvey 1991).
- An additional force component proportional to $\partial^2\varepsilon/\partial z^2$.
- A geometrical averaging approach that corrects the effective area-averaged void fraction when changes occur on the scale of the particles (Singh & Joseph 1991).

These theories have been shown to be closely related and approximately compatible. They fit a range of decompression wave data quite well but show significant deviations (which we have not tried to fit empirically) at high values of density ratio ($\rho_s/\rho_f \geqslant 10$) and low $\mathrm{Re}_\infty$ ($\leqslant 100$). They have not been used in this paper to predict the transition to three-dimensional behavior that occurs with small particles and small density ratios, roughly corresponding to the range of "particulate" or non-bubbling fluidization, though Singh & Joseph (1991) have used a similar approach to develop a criterion resembling that of Foscolo & Gibilaro (1984).

The decompression wave data, and subsidiary experiments to measure forces on particles at interfaces, provide less favorable support for the hypothesis of an "effective compressibility" or a force component that is proportional to the void fraction gradient, $\partial\varepsilon/\partial z$. Although, mathematically, such an effect can qualitatively explain the results, the required compressibility would be extraordinarily sensitive to void fraction. In a fluidized bed, however, in which more velocity fluctuations are likely to build up than are induced in a decompression wave, there may be an additional mechanism for such an effect, as envisaged by Batchelor (1988).

One-dimensional decompression waves occur for a range of physical properties generally associated with "aggregative", "bubbling" or "slugging" fluidization and could represent the "rainoff" process at the bottom of a slug of particles in such a system. The three-dimensional instability that is observed, for example with glass beads of diameter less than about 4 mm in water, could be related to the mechanism that breaks up "bubbles" in "particulate" fluidized beds. Such phenomena were not predicted from the analysis in this paper. Nor do we have an explanation for why [35] appears to describe the decompression wave speed when $j_{fa}/j_{mf} \to 1$, *even when the waves*

*appear three-dimensional*, as reported in several papers by Gibilaro *et al.* (1989, 1990). Perhaps the initial peeling off of particles from the compressed stack is governed by some local phenomena that are independent of the structure of the flow below.

In the comparisons that we have presented between data and predictions, the "theoretical" values are entirely theoretical (i.e. calculated values of $j_{mf}$ and $v_\infty$ are used) while experimental data are reduced using measured values of $j_{mf}$. In some cases this makes little difference; e.g. for 6 mm lead glass in water we measured $j_{mf} = 54.9$ mm/s and calculated 54.6 mm/s and for 8 mm soda glass we measured $j_{mf} = 63.5$ mm/s and calculated 61 mm/s. However, for 420 $\mu$m lead glass in water (figure 31) we measured $j_{mf} = 3.7$ mm/s and computed 2.1 mm/s. Attempts to "correct" the data in figure 31 by mixing theoretical and experimental values merely make the comparison worse and do not remove the basic qualitative disagreements. For 2.44 mm lead shot in water we measured $j_{mf} = 84$ mm/s and computed 70.2 mm/s; if this discrepancy is used to change the scale on the abscissa in figure 32, the agreement with theory is much improved at lower wave speeds. A similar "correction" of about 20% could be applied to figure 33, moving the data between the theoretical curves represented there. In no case, however, do we have experimental values of $v_\infty$ to justify changes in the scale of the ordinate. All in all, we believe the comparisons we have shown are the fairest method of representation. Errors as high as 50% in predicting $j_{mf}$ at low Re are indicative of the state-of-the-art and argue against expectations of greater precision in representing decompression wave results. Sources of uncertainty include non-uniformity, out-of-roundness and roughness of the particles and variations in void fraction in a packed bed, depending on how it is created.

*Acknowledgement*—This work was supported by the U.S. Department of Energy, Contract No. DE-FG02-86ER13528, administered by Dr Oscar Manley.

## REFERENCES

BATCHELOR, G. K. 1988 A new theory of the instability of a uniform fluidized bed. *J. Fluid Mech.* **193,** 75–110.

BIRD, R. B., STEWART, W. E. & LIGHTFOOT, E. N. 1960 *Transport Phenomena.* Wiley, New York.

BUYSMAN, P. J. & PEERSMAN, G. A. L. 1967 Stability of ceilings in a fluidized bed. In *Proceedings of the International Symposium on Fluidization* (Edited by DRINKENBURG, A. A. H.). Netherlands Univeristy Press, Amsterdam.

FOSCOLO, P. U. & GIBILARO, L. G. 1984 A fully predictive criterion for the transition between particulate and aggregative fluidization. *Chem. Engng Sci.* **39,** 1667–1675.

GIBILARO, L. G., DIFELICE, R., WALDRAM, S. P. & FOSCOLO, P. U. 1985 Generalized friction factor and drag coefficient correlations for fluid–particle interactions. *Chem. Engng Sci.* **40,** 1817–1823.

GIBILARO, L. G., DIFELICE, R., HOSSAIN, I. & FOSCOLO, P. U. 1989 The experimental determination of one-dimensional wave velocities in liquid fluidized beds. *Chem. Engng Sci.* **44,** 101–107.

GIBILARO, L. G. DIFELICE, R. & FOSCOLO, P. U. 1990 Added mass effects in fluidized beds: application of the Guerst–Wallis analysis of inertial coupling in two-phase flow. *Chem. Engng Sci.* **45,** 1561–1565.

HARVEY, S. P. 1991 A study of forces acting on particles in fluidized beds and their implications for bed stability. M.S. Thesis, Thayer School of Engineering, Dartmouth College, Hanover, NH.

JACKSON, R. 1963 The mechanics of fluidized beds. Part I: the stability of the state of uniform fluidization; Part II: the motion of fully developed bubbles. *Trans. Instn Chem. Engrs* **41,** 13–28.

MURRAY, J. D. 1965 On the mathematics of fluidization, Part 1: fundamental equations and wave propagation. *J. Fluid Mech.* **21,** 465–493.

RICHARDSON, J. F. & ZAKI, W. N. 1954 Sedimentation and fluidization, Part 1. *Trans. Instn Chem. Engrs* **32,** 35–53.

ROWE, P. N. & HENWOOD, G. A. 1961 Drag forces in a hydraulic model of a fluidized bed—Part 1. *Trans. Instn Chem. Engrs* **39,** 43–54.

SIMPSON, H. C. & RODGER, B. W. 1961 The fluidization of light solids by gases under pressure and heavy solids by water. *Chem. Engng Sci.* **16,** 153–180.

SINGH, P. & JOSEPH, D. D. 1991 Dynamics of fluidized suspensions of spheres of finite size. Presented at the *IUTAM Symp. on Mechanics of Fluidized Beds*, Stanford Univ., CA, July.

WALLIS, G. B. 1962, One-dimensional waves in two-component flow (with particular reference to the stability of fluidized beds). UKAEA Report AEEW-R162.

WALLIS, G. B. 1969 *One-dimensional Two-phase Flow*. McGraw-Hill, New York.

WALLIS, G. B. 1977 A simple correlation for fluidization and sedimentation. *Trans. Instn Chem. Engrs* **55**, 74–75.

WALLIS, G. B. 1989 Inertial coupling in two-phase flow: macroscopic properties of suspensions in an inviscid fluid. *Multiphase Sci. Technol.* **5**, 239–361.

WALLIS, G. B. 1990 On Geurst's equations for inertial coupling in two-phase flow. In *Two-phase Flows and Waves* (Edited by JOSEPH, D. D. & SCHAEFFER, D. G.), pp. 150–164. Springer-Verlag, New York.

WEN, C. Y. & YU, Y. H. 1966 Mechanics of fluidization. *Chem. Engng Proc. Symp.* **62**, 100–111.